

Sterically Demanding, Sulfonated, Triarylphosphines: Application to Palladium-Catalyzed Cross-Coupling, Steric and Electronic Properties, and Coordination Chemistry

Lucas R. Moore, Elizabeth C. Western, Raluca Craciun, Jason M. Spruell, David A. Dixon,*
Kevin P. O'Halloran, and Kevin H. Shaughnessy*

Department of Chemistry and Center for Green Manufacturing, The University of Alabama,
Tuscaloosa, Alabama 35487-0336

Received August 28, 2007

Tri(2,4-dimethyl-5-sulfonatophenyl)phosphine trisodium (TXPTS·Na₃) and tri(4-methoxy-2-methyl-5-sulfonatophenyl)phosphine trisodium (TMAPTS·Na₃) both provide more active catalysts for Suzuki and Sonogashira couplings of aryl bromides in aqueous solvents than tri(3-sulfonatophenyl)phosphine trisodium (TPPTS·Na₃). In the Heck coupling, TXPTS·Na₃ provides the most effective catalyst system. Cone angles determined from DFT-optimized structures show that both TXPTS·Na₃ (206°) and TMAPTS·Na₃ (208°) are significantly larger than TPPTS·Na₃ (165°). The identity of the counterion had a significant effect on the calculated cone angles for these ligands. The electronic properties of these ligands determined by the CO stretching frequencies of *trans*-RhL₂(Cl)CO complexes were identical, although calculated electronic parameters suggest subtle differences between these ligands. Similar to TPPTS·Na₃, both TXPTS·Na₃ and TMAPTS·Na₃ react with Pd(OAc)₂ in aqueous solvents to give L_nPd⁰ complexes and the corresponding phosphine oxide. The reduction of palladium(II) by TXPTS·Na₃ is significantly slower than is seen with TMAPTS·Na₃ or TPPTS·Na₃ at room temperature. Evidence of palladacycle complexes derived from TXPTS·Na₃ and TMAPTS·Na₃ by activation of an *ortho*-methyl substituent was also observed in ligand coordination studies and under catalytic reaction conditions.

Introduction

Water is an attractive solvent for organic synthesis due to its low toxicity, nonflammability, low cost, and limited environmental impact.^{1,2} In addition, the use of an aqueous–organic biphasic solvent system in conjunction with a water-soluble catalyst provides a route to recover and recycle the catalyst from organic product streams. Water-soluble catalyst systems also provide efficient methods to modify hydrophilic substrates, such as nucleosides and peptides.^{3–8} A variety of metal-catalyzed reactions can be successfully run in aqueous solvent systems, with palladium-catalyzed cross-couplings being one of the most widely developed.^{9,10} The first example of aqueous-phase, palladium-catalyzed cross-coupling was reported by Casalnuovo,¹¹ who used Pd(TPPMS·Na)₃ (TPPMS·Na = diphenyl(3-sulfonatophenyl)phosphine sodium, Figure 1) as the cata-

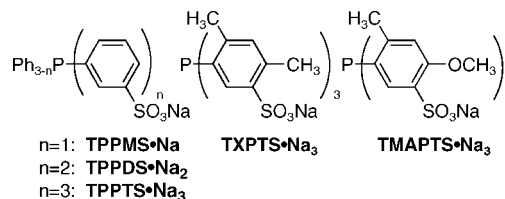


Figure 1. Sulfonated triarylphosphines.

lyst. This catalyst system gave good yields with aryl iodides and a few examples of aryl bromides, but required high catalyst loadings. Since Casalnuovo's initial report, a wide variety of water-soluble phosphine ligands have been developed.⁹ Like TPPMS·Na, nearly all of these ligands are triarylphosphines substituted with a variety of anionic, cationic, or neutral hydrophilic substituents. Catalysts derived from these ligands generally give good yields with aryl iodides and are effective in some cases with aryl bromides at elevated temperatures.

Over the past decade, sterically demanding and electron-rich ligands have been shown to give highly effective catalysts for cross-coupling reactions under mild conditions. Bulky, electron-rich ligands, such as tri-*tert*-butylphosphine,^{12–15} 2-biphenyldialkylphosphines,^{16–19} and *N*-heterocyclic carbenes,^{20–22} provide

* Corresponding authors. E-mail: dadixon@bama.ua.edu; kshaughn@bama.ua.edu.

- (1) Li, C.-J.; Chen, L. *Chem. Soc. Rev.* **2006**, *35*, 68–82.
- (2) Li, C.-J. *Chem. Rev.* **2005**, *105*, 3095–3165.
- (3) Western, E. C.; Daft, J. R.; Johnson, E. M., II; Gannett, P. M.; Shaughnessy, K. H. *J. Org. Chem.* **2003**, *68*, 6767–6774.
- (4) Capek, P.; Pohl, R.; Hocek, M. *Org. Biomol. Chem.* **2006**, *4*, 2278–2284.
- (5) Collier, A.; Wagner, G. *Org. Biomol. Chem.* **2006**, *4*, 4526–4532.
- (6) Dibowski, H.; Schmidtchen, F. P. *Angew. Chem., Int. Ed.* **1998**, *37*, 476–478.
- (7) Dibowski, H.; Schmidtchen, F. P. *Tetrahedron Lett.* **1998**, *39*, 525–528.
- (8) Thoresen, L. H.; Jiao, G.-S.; Haaland, W. C.; Metzker, M. L.; Burgess, K. *Chem.—Eur. J.* **2003**, *9*, 4603–4610.
- (9) Shaughnessy, K. H.; DeVasher, R. B. *Curr. Org. Chem.* **2005**, *9*, 585–604.
- (10) Shaughnessy, K. H. *Eur. J. Org. Chem.* **2006**, 1827–1835.
- (11) Casalnuovo, A. L.; Calabrese, J. C. *J. Am. Chem. Soc.* **1990**, *112*, 4324–4330.

(12) Hartwig, J. F.; Kawatsura, M.; Hauck, S. I.; Shaughnessy, K. H.; Alcazar-Roman, L. M. *J. Org. Chem.* **1999**, *64*, 5575–5580.

(13) Littke, A. F.; Dai, C.; Fu, G. C. *J. Am. Chem. Soc.* **2000**, *122*, 4020–4028.

(14) Littke, A. F.; Fu, G. C. *J. Am. Chem. Soc.* **2001**, *123*, 6989–7000.

(15) Littke, A. F.; Schwarz, L.; Fu, G. C. *J. Am. Chem. Soc.* **2003**, *124*, 6343–6348.

(16) Burgos, C. H.; Barder, T. E.; Huang, X.; Buchwald, S. L. *Angew. Chem., Int. Ed.* **2006**, *45*, 4321–4326.

active catalysts for coupling of aryl bromides and chlorides at ambient temperatures in many cases. Steric bulk is necessary to promote the formation of coordinatively unsaturated palladium species, which are the presumed catalytically active species. Electron-rich ligands help to promote oxidative addition, which is particularly important when using less reactive aryl bromide or chloride substrates. Ligand size appears to be the critical factor in determining catalyst activity in cross-coupling reactions of aryl bromides, while electron-donating ability becomes more important with the less reactive aryl chlorides.^{23,24}

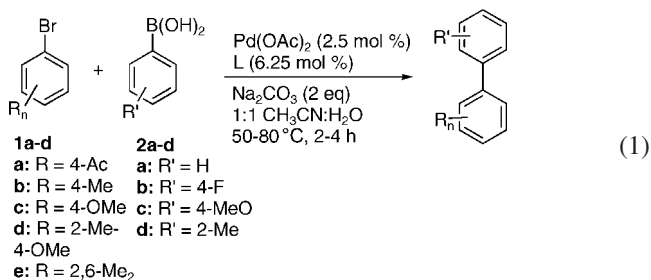
Only recently have hydrophilic ligands with large steric demand and strong electron-donating ability been applied to aqueous-phase cross-coupling reactions. Hydrophilic trialkylphosphines^{25,26} and 2-phosphinobiphenyl ligands^{27–29} have been shown to give highly effective catalysts for cross-coupling reactions of aryl bromides and chlorides. Dialkylphosphinonic acids have also been applied to aqueous-phase cross-coupling of aryl bromides and chlorides, although at elevated temperatures.^{30–34} Tri-(2,4-dimethyl-5-sulfonatophenyl)phosphine trisodium (TXPTS·Na₃), a sterically demanding analogue of TPPTS·Na₃, was first prepared by Bakos and co-workers.³⁵ We have previously communicated the use of TXPTS·Na₃ and TMAPTS·Na₃ (tri-(4-methoxy-2-methyl-5-sulfonatophenyl)phosphine trisodium) in aqueous Heck and Suzuki couplings.³⁶ Herein we report the utility of TXPTS·Na₃ and TMAPTS·Na₃ as ligands in palladium-catalyzed coupling reactions, their steric and electronic properties, and the coordination chemistry of these ligands with palladium.

Results

Ligand Synthesis. The syntheses of TXPTS·Na₃³⁵ and TMAPTS·Na₃³⁶ have previously been reported. Both ligands are prepared by sulfonation of the corresponding phosphines (tri-(2,4-dimethylphenyl)phosphine (TXP) and tri(4-methoxy-2-methylphenyl)phosphine (TMAP)), which can be readily

prepared by condensation of the corresponding Grignard reagents with PCl₃, with fuming sulfuric acid at room temperature. The electron-releasing substituents on TXP and TMAP make these phosphines more readily sulfonated than triphenylphosphine, which requires long reaction times and/or harsh conditions to achieve complete sulfonation.³⁷ These harsh reaction conditions result in competitive oxidation of the phosphorus center during the sulfonation of triphenylphosphine. In contrast, TXP and TMAP can be readily sulfonated in a few hours at room temperature to give the desired ligands in good yield with little oxide impurity.³⁸

Catalytic Applications. TXPTS·Na₃ and TMAPTS·Na₃ both gave effective catalysts for the Suzuki coupling of aryl bromides at 50 °C.³⁶ Catalysts derived from these ligands were moderately more active than the catalyst derived from TPPTS·Na₃. Using 0.05 mol % of a catalyst derived from the ligand and Pd(OAc)₂ (2.5:1 L:Pd) for the coupling of 4-bromotoluene and phenylboronic acid, the catalyst derived from TXPTS·Na₃ and TMAPTS·Na₃ gave 78% and 68% yields, respectively, as determined by GC after 2.5 h. The catalyst derived from TPPTS·Na₃ had given only a 48% yield over the same time period. Pd(OAc)₂ without ligand gave no conversion under these conditions. The TXPTS·Na₃/Pd(OAc)₂ catalyst system also gave slow conversion for the coupling of 4-bromotoluene and phenyl boronic acid at room temperature, requiring 70 h to give an 87% yield of product using 2.5 mol % catalyst. Both the TXPTS·Na₃- and TMAPTS·Na₃-derived catalysts gave excellent yields in the Suzuki coupling of a variety of aryl bromides (eq 1, Table 1). Electron-deficient and -neutral aryl halides gave excellent yields at 50 °C (entries 1–5). 4-Methoxy-substituted aryl bromides also gave excellent yields at 50 °C with TMAPTS·Na₃, but required 80 °C with TXPTS·Na₃. Couplings to give *ortho*-substituted biphenyls gave good yields at 50 °C, but the yields could be improved by running the reaction at 80 °C (i.e., entries 10, 11).



Catalysts derived from TXPTS·Na₃ and TMAPTS·Na₃ also proved to be superior to the catalyst derived from TPPTS·Na₃ for the Sonogashira coupling of aryl bromides at 50 °C. In the coupling of 4-bromotoluene and phenylacetylene, the catalysts derived from TXPTS·Na₃ and TMAPTS·Na₃ gave 81% and 92% yield, respectively (3 mol % Pd(OAc)₂, 8 mol % ligand, 5 h). The TPPTS·Na₃-derived catalyst gave only a 47% yield of diphenylacetylene under identical conditions. In the absence of ligand, no product formation occurred. Significantly, the reaction proceeded in the absence of copper cocatalyst. In fact, the use of CuI (2 mol %) resulted in lower yields due to competitive homodimerization of phenylacetylene. Excellent yields were obtained in the coupling of electron-deficient aryl halides with phenylacetylene using both TXPTS·Na₃ and

(17) Barder, T. E.; Walker, S. D.; Martinelli, J. R.; Buchwald, S. L. *J. Am. Chem. Soc.* **2005**, *127*, 4685–4696.

(18) Walker, S. D.; Barder, T. E.; Martinelli, J. R.; Buchwald, S. L. *Angew. Chem., Int. Ed.* **2004**, *43*, 1871–1876.

(19) Milne, J. E.; Buchwald, S. L. *J. Am. Chem. Soc.* **2004**, *126*, 13028–13032.

(20) Viciu, M. S.; Navarro, O.; Germaneau, R. F.; Kelly, R. A., III; Sommer, W.; Marion, N.; Stevens, E. D.; Cavallo, L.; Nolan, S. P. *Organometallics* **2004**, *23*, 1629–1635.

(21) Hadei, N.; Kantchev, E. A. B.; O'Brien, C. J.; Organ, M. G. *Org. Lett.* **2005**, *7*, 3805–3807.

(22) Marion, N.; Navarro, O.; Mei, J.; Stevens, E. D.; Scott, N. M.; Nolan, S. P. *J. Am. Chem. Soc.* **2006**, *128*, 4101–4111.

(23) DeVasher, R. B.; Spruell, J. M.; Dixon, D. A.; Broker, G. A.; Griffin, S. T.; Rogers, R. D.; Shaughnessy, K. H. *Organometallics* **2005**, *24*, 962–971.

(24) Hill, L. L.; Moore, L. R.; Huang, R.; Craciun, R.; Vincent, A. P.; Dixon, D. A.; Chou, J.; Woltermann, C. J.; Shaughnessy, K. H. *J. Org. Chem.* **2006**, *71*, 5117–5125.

(25) DeVasher, R. B.; Moore, L. R.; Shaughnessy, K. H. *J. Org. Chem.* **2004**, *69*, 7919–7927.

(26) Shaughnessy, K. H.; Booth, R. S. *Org. Lett.* **2001**, *3*, 2757–2759.

(27) Nishimura, M.; Ueda, M.; Miyaura, N. *Tetrahedron* **2002**, *58*, 5779–5787.

(28) Konovets, A.; Penciu, A.; Framery, E.; Percina, N.; Goux-Henry, C.; Sinou, D. *Tetrahedron Lett.* **2005**, *46*, 3205–3208.

(29) Anderson, K. W.; Buchwald, S. L. *Angew. Chem., Int. Ed.* **2005**, *44*, 6175–6177.

(30) Wolf, C.; Lerebours, R. *J. Org. Chem.* **2003**, *68*, 7551–7554.

(31) Wolf, C.; Lerebours, R. *Org. Lett.* **2004**, *6*, 1147–1150.

(32) Wolf, C.; Lerebours, R. *Org. Biomol. Chem.* **2004**, *2*, 2161–2164.

(33) Lerebours, R.; Wolf, C. *Synthesis* **2005**, 2287–2292.

(34) Wolf, C.; Ekoue-Kovi, K. *Eur. J. Org. Chem.* **2006**, 1917–1925.

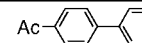
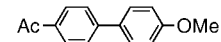
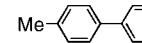
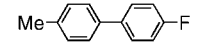
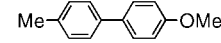
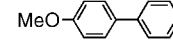
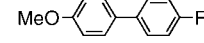
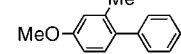
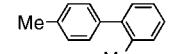
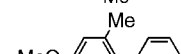
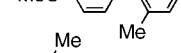
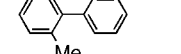
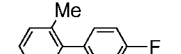
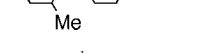
(35) Gulyás, H.; Szöllösy, Á.; Hanson, B. E.; Bakos, J. *Tetrahedron Lett.* **2002**, *43*, 2543–2546.

(36) Moore, L. R.; Shaughnessy, K. H. *Org. Lett.* **2004**, *6*, 225–228.

(37) Bartik, T.; Bartik, B.; Hanson, B. E.; Glass, T.; Bebout, W. *Inorg. Chem.* **1992**, *31*, 2667–2670.

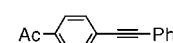
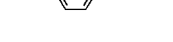
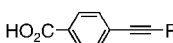

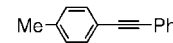
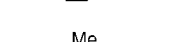
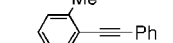
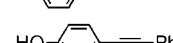
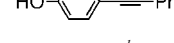
(38) TPPTS·Na₃ purchased from Strem Chemical has 10–15% oxide impurity, while TXPTS·Na₃ is available in 97% purity.

Table 1. Suzuki Coupling of Aryl Bromides Using TXPTS·Na₃ and TMAPTS·Na₃

entry	1	2	L ^a	T (°C)	product	yield (%) ^b
1	1a	2a	A	50		91
2	1a	2c	B	50		99
3	1b	2a	B	50		97
4	1b	2b	A	50		94
5	1b	2c	A	50		92
6	1c	2a	A	80		99
7	1c	2b	B	50		97
8	1d	2a	A	50		88
9	1b	2d	B	80		86
10	1d	2d	A	50		75
11	1d	2d	A	80		92
12	1d	2d	B	80		91
13	1e	2a	A	80		84
14	1e	2b	B	50		87

^a A = TXPTS·Na₃, B = TMAPTS·Na₃. ^b Average isolated yield of at least two runs. Reactions were run until judged complete by GC (typically 2–4 h). Reaction times were not optimized.

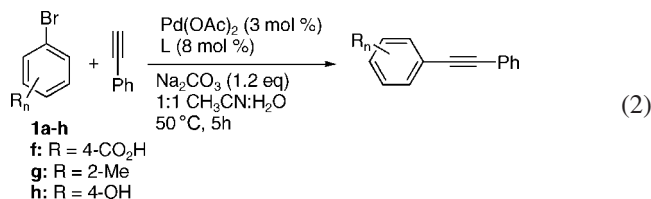
Table 2. Sonogashira Coupling of Aryl Bromides Using TXPTS·Na₃ and TMAPTS·Na₃

entry	ArBr	L ^a	product	yield (%) ^b
1	1a	A		97
2	1a	B		94
3	1f	A		99
4	1f	B		99
5	1b	A		74
6	1b	B		74
7	1g	A		73
8	1g	B		81
9	1h	A		0

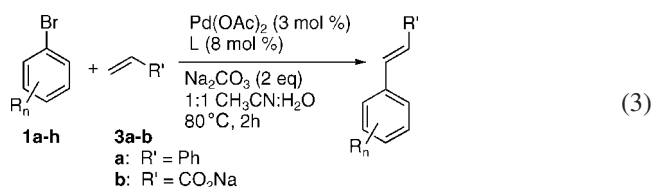
^a A = TXPTS·Na₃, B = TMAPTS·Na₃. ^b Average isolated yield of at least two runs. Reaction times were not optimized.

TMAPTS·Na₃ (eq 2, Table 2). Bromotoluene derivatives gave good yields of coupled product, although lower than those achieved with activated aryl bromides. 4-Bromophenol, an electron-rich aryl halide, was unreactive under these reaction conditions. Attempted couplings with aliphatic alkynes, such as 1-hexyne, were unsuccessful with this catalyst system in both the presence and absence of catalytic CuI.

In the Heck coupling of aryl bromides, TXPTS·Na₃ gave a more active catalyst than either TMAPTS·Na₃ or TPPTS·Na₃. In the coupling of 4-bromotoluene and styrene at 80 °C using



2.5 mol % Pd(OAc)₂ (2.5:1 L:Pd), the catalyst derived from TXPTS·Na₃ gave a 77% yield of 4-methylstilbene after 2 h. The TMAPTS·Na₃-derived catalyst gave only a 40% yield, while the catalyst formed from TPPTS·Na₃ gave only a 28% yield of the stilbene product. In the absence of ligand, no product formation was observed. Good to excellent yields were obtained from the coupling of aryl bromides and styrene or sodium acrylate (eq 3, Table 3). Styrene consistently gave higher yields of coupling products than did sodium acrylate. The choice of aryl bromide did not have a significant effect on the reaction yield.



Mercury Poisoning Test. In an effort to determine whether the active species was a soluble palladium/phosphine complex or heterogeneous palladium particles, a mercury test was performed.³⁹ The rate of coupling of 4-bromotoluene and phenylboronic acid catalyzed by TXPTS/Pd(OAc)₂ (1.25 mol% Pd, 2.5:1 L:Pd) in 1:1 acetonitrile/water at 50 °C in the presence and absence of mercury were compared. In one sample, the mercury (0.5 mL) was added to the dry reagents prior to the addition of solvent and the aryl halide. These conditions test the ability to form the active species in the presence of Hg⁰. In a second sample, the reaction was allowed to proceed for 15 min to allow time for the active catalyst to form before the mercury was added. Under these conditions, the stability of the preformed active species in the presence of Hg⁰ is determined. Figure 2 shows the reaction profiles for the two mercury-containing reactions and a control with no mercury. The reaction profiles are similar for all three reactions. The mercury-containing reactions have slightly lower conversions than the control after 75 min, but the difference is small. Up to this point, the reaction profiles are nearly identical. These results are consistent with a homogeneous, molecular species being the true catalyst rather than heterogeneous palladium particles or colloids.

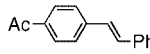
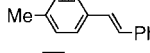
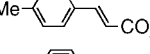
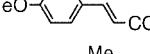
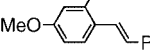
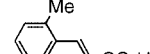
DFT-Calculated Ligand Structures. In order to gain a fuller understanding of why TXPTS·Na₃ and TMAPTS·Na₃ tend to give more effective catalysts than TPPTS·Na₃, the steric and electronic properties of these ligands were determined by experimental and computational methods. We have previously shown that the geometries and frequencies of transition metal complexes^{23,40} can be predicted reliably at the local density functional theory (LDFT) level.⁴¹ Geometries of Pd⁰L₂ and Pd⁰L complexes were optimized at the LDFT level with the polarized

(39) Widegren, J. A.; Finke, R. G. *J. Mol. Catal. A: Chem.* **2003**, *198*, 317–341.

(40) Sosa, C.; Andzelm, J.; Elkin, B. C.; Wimmer, E.; Dobbs, K. D.; Dixon, D. A. *J. Phys. Chem.* **1992**, *96*, 6630–6636.

(41) Parr, R. G.; Yang, W. *Density-Functional Theory of Atoms and Molecules*; Oxford University Press: New York, 1989.

Table 3. Heck Coupling of Aryl Bromides Using TXPTS·Na₃

entry	1	3	product	yield (%) ^a
1	1a	3a		94
2	1b	3a		90
3	1b	3b ^b		81
4	1c	3b ^b		79
5	1d	3a		78
6	1g	3b ^b		82

^a Average isolated yield of at least two runs. Reactions were run for 2 h and were not optimized. ^b Crude product was acidified with H₂SO₄ prior to isolation.

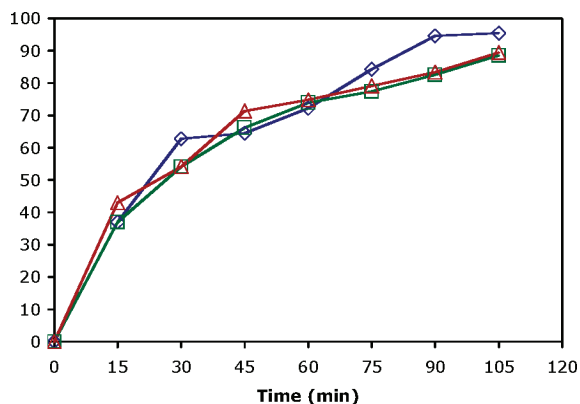


Figure 2. Reaction profile in the mercury poisoning experiment in the Suzuki coupling of 4-bromotoluene and phenylboronic acid catalyzed by TXPTS/Pd(OAc)₂. Control with no Hg⁰ (diamonds), Hg⁰ added initially (squares); Hg⁰ added after 15 min (triangles).

double- ζ DZVP2 basis set on all atoms except Pd.⁴² We used the Stuttgart relativistic pseudopotential and the associated basis set for Pd⁴³ with 28 electrons in the core of the ECP. The basis set for Pd was contracted to [6s5p3d]. The LDFT calculations were done with the potential fit of Vosko, Wilk, and Nusair for the correlation functional⁴⁴ and the exchange functional of Slater.⁴⁵ The calculations were done with the program Gaussian03⁴⁶ on Cray XD-1 and Silicon Graphics Altix computers at the Alabama Supercomputing Center.

Four optimized geometries were calculated for each sulfonated ligand and their corresponding Pd complexes: the trianionic ligand with no counterion (L³⁻), the neutral trisulfonic acid (L·H₃) with and without intramolecular H-bonding of the SO₃H groups, and trisodium salt of the ligand (L·Na₃). Each of the PdL complex calculations started with a zerovalent

palladium center. The structures of the H⁺ and Na⁺ adducts of the trianionic ligands were calculated to compensate for the large charge repulsions that would be present in the gas-phase structures of the polyanions. In addition, structures of palladium complexes of a number of neutral structures were calculated to determine the effect of the sulfonate group on the ligand geometries.

The structures of the PdL complexes are strongly affected by the addition of Na⁺ or H⁺ to the sulfonate ion (Figure 3). The structure of Pd(TPPTS³⁻) has C–P–C and Pd–P–C bond angles near 109°, showing a nearly perfect tetrahedral geometry around the phosphorus atom (Figure 4, Table 4). The dihedral angle between the Pd–P bond and the plane of the aromatic ring (Pd–P–C–C) is –60°. This arrangement gives an open structure that maximizes the distance between the negatively charged sulfonate groups. The Pd–P bond length for the trianionic complex is 2.149 Å. When the charge on the sulfonate groups is balanced with a proton or sodium ion, the geometry of the ligand changes significantly. In the most stable sulfonic acid structure, the sulfonic acid groups are held in close proximity by intramolecular hydrogen bonding. The aryl rings are pulled back away from the Pd, resulting in a larger Pd–C–P angle compared to the trianionic complex. The Pd–P–C–C torsion angle is decreased to –46°, which brings the aryl rings closer to parallel with the Pd–P bond. The Pd–P bond of the TPPTS·H₃ is 2.114 Å, which is shorter than the trianion structure. We attempted to optimize a structure without H-bonding between the SO₃H groups, but it collapsed to the H-bonded structure. When sodium counterions are added to each sulfonate group, the structure again becomes more compact due to each sodium ion coordinating to two sulfonate groups (Figure 3C). Again the Pd–P–C angle increases and two of the phenyl rings rotate so that they are more parallel with the Pd–P bond (Pd–P–C–C = –14°, –32°, and –62°). The Pd–P bond of the Pd(TPPTS·Na₃) complex is longer than that of the TPPTS³⁻ complex by 0.035 Å.

The Pd–P bond distances for the TXPTS complexes are longer than were observed for the TPPTS complexes, likely due to the steric repulsion between the Pd center and the *ortho*-methyl groups. The C–P–C angle of the TXPTS³⁻ structure (109°) is similar to that of the TPPTS³⁻ complex, while the torsion angle of the TXPTS³⁻ complex (–52°) is smaller than that of Pd(TPPTS³⁻). The sulfonic acid structure (TXPTS·H₃) has strong hydrogen bonds between the SO₃H groups, leading to the smallest C–P–C angle for this ligand and shortest Pd–P bond distance (Figure 5B). Consequently the smallest torsion angle for the TXPTS structures is found for the H-bonded sulfonic acid structure. The sulfonic acid structure with no hydrogen bonding between the sulfonic acid groups (Figure 5C) is 7.8 kcal/mol higher in energy than the structure with hydrogen bonding. In the free ligand, the H-bonded structure is 18.0 kcal/mol more stable than the non-H-bonded structure. The Pd–P bond length is longest for the non-hydrogen-bonded TXPTS·H₃ structure and, in fact, is the longest P–C bond predicted for any of the structures. The structure with three Na⁺ counterions (Figure 5D) has a smaller CPC angle than the trianion, but there is only a small decrease in the torsion angle compared to that seen for TPPTS³⁻. Again, the Pd–P bond becomes longer when sodium ions are added to the sulfonate groups, although the increase is less than was seen for the TPPTS system.

The Pd(TMAPTS³⁻) structure is nearly identical to that of Pd(TXPTS³⁻), except that the Pd–P bond is shorter.⁴⁷ Addition

(42) Godbout, N.; Salahub, D. R.; Andzelm, J.; Wimmer, E. *Can. J. Chem.* **1992**, *70*, 560–571.

(43) Küchle, W.; Dolg, M.; Stoll, H.; Preuss, H. *J. Chem. Phys.* **1994**, *100*, 7535–7542.

(44) Vosko, S. H.; Wilk, L.; Nusair, M. *Can. J. Phys.* **1980**, *58*, 1200–1211.

(45) Slater, J. C. *Phys. Rev.* **1951**, *81*, 385–390.

(46) Frisch, M. J.; et al. *Gaussian 03, Revision C.02*; Gaussian Inc., 2004.

(47) Models of the trianion, sulfonic acid, and sodium salts of the PdL complexes are included in the Supporting Information.

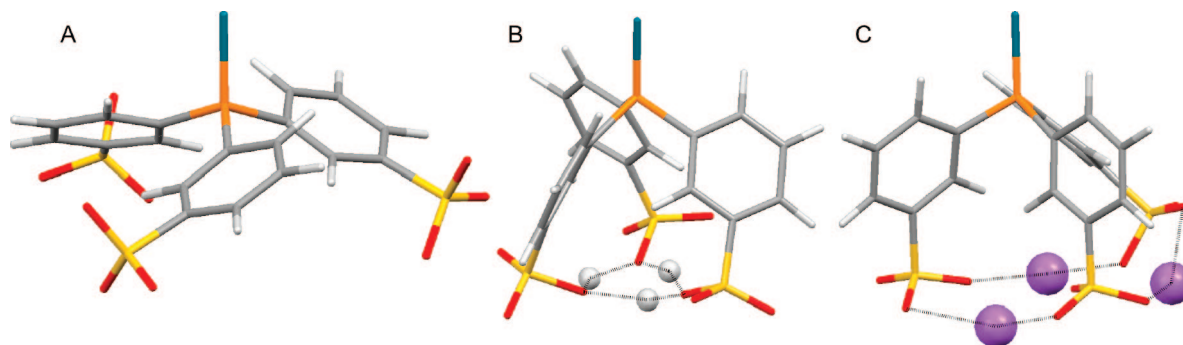


Figure 3. Cylindrical bond models of calculated Pd(TPPTS³⁻) (A), Pd(TPPTS·H₃) (B), and Pd(TPPTS·Na₃) (C) structures. Carbon, gray; hydrogen, white; phosphorus, orange; sulfur, yellow; oxygen, red; palladium, blue; sodium, purple.

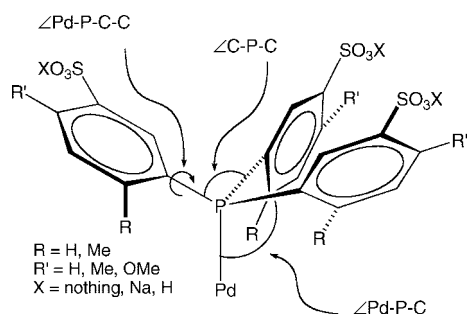


Figure 4. Key geometry parameters summarized in Table 4.

of sodium ions results in a similar structural change to that seen with the TPPTS system. The sodium ions pull the sulfonate groups closer together as seen from the increase in the Pd–P–C angle and decrease in the C–Pd–C angle. Two of the three aryl rings show decreased torsional angles, although this decrease is less dramatic than in the case of TPPTS. This arrangement allows the sodium ions to each coordinate to two sulfonate groups. Protonation of the sulfonate groups gives a structure that is similar to the Pd(TPPTS·H₃) or Pd(TXPTS·H₃) structures. The structure is again pulled back by strong SO₃H–SO₃H hydrogen bonds. The Pd–P bond is shortest for the hydrogen-bonded protonated ligand and longest for the trianion as found for the other structures. The hydrogen-bonded sulfonic acid structure is more stable than the non-H-bonded structure when bonded to Pd by 5.5 kcal/mol. In the free ligand, the H-bonded structure is more stable by 3.6 kcal/mol.

The introduction of *ortho*-methyl substituents in the ligands results in significant steric congestion around the metal. As a result, TXPTS and TMAPTS have close contacts between hydrogen atoms on each of the *ortho*-methyl groups and the palladium center. The closest contacts ranged from 2.35 to 2.60 Å (Table 4). These contacts are smaller than the sum of the van der Waals radii for H and Pd (2.89 Å), suggesting that there are agostic interactions in these complexes. The neutral analogues of these ligands (P(*o*-tol)₃, TXP, and TMAP) also have close contacts of 2.35–2.36 Å, and trimesitylphosphine has an even closer contact of 2.13 Å.

The bond dissociation energies were calculated at the LDA geometries with the B3LYP exchange–correlation functional^{48,49} and the polarized Ahlrichs triple- ζ basis set⁵⁰ on the nonmetal atoms and the above Stuttgart basis set and ECP on Pd. As

found previously, the bond energies for the compounds defined as $BDE = E_{Pd} + E_L - E_{PdL}$ cover a small range between 32 and 38 kcal/mol except for the P(2,4-*t*-Bu₂C₆H₃)₃ ligand (Table 4). The latter compound has a very large steric hindrance due to the *tert*-butyl groups in the *ortho*-position that largely covers the lone pair on the P, making it quite inaccessible to the Pd. The low BDE is consistent with the large cone angle and the long Pd–P bond. The TPPTS, TXPTS, and TMAPTS ligands show some variations in the BDE due to the presence of counterions. The largest effect is found for TXPTS·H₃, where the difference in energies between the H-bonded and non-H-bonded structures is about 10 kcal/mol. The Pd–P bond energy is largest for PPh₃ followed by the three anionic ligands. Alkyl substituents on PPh₃ lower the BDE by about 5 kcal/mol for TMAP, TXP, and P(*o*-tol)₃ with a lowering of about 11 kcal/mol for P(Mes)₃. As noted above, the *tert*-butyl substituents in P(2,4-*t*-Bu₂C₆H₃) lower the BDE by almost 30 kcal/mol.

Experimental and Calculated Steric and Electronic Ligand Parameters. The steric demand of phosphines can be expressed by a number of parameters.⁵¹ The most commonly used steric descriptor is the cone angle concept developed by Tolman.⁵² Tolman utilized plastic CPK models in order to determine his cone angle values. He assumed a static M–P bond distance of 2.28 Å and placed the phosphine substituents to give the minimum cone angle. Despite this somewhat simplistic approach, the Tolman cone angles have proven to correlate well with catalyst activity and coordination chemistry in a variety of systems. Cone angles can also be obtained from solid-state structures using methods developed by Mingos and co-workers.⁵³ Using this approach, Mingos was able to obtain cone angles for a large number of structures that had been deposited in crystallographic databases. This data provided a picture of the range of cone angles for a given ligand for a variety of metal complex types. Another approach to calculate cone angles of phosphine ligands is the use of solid angles.^{54,55} An efficient

(51) White, D.; Coville, N. J. *Adv. Organomet. Chem.* **1994**, *36*, 95–158.

(52) Tolman, C. A. *Chem. Rev.* **1977**, *77*, 313–348.

(53) Müller, T. E.; Mingos, D. M. P. *Transition Met. Chem.* **1995**, *20*, 533–539.

(54) Hirota, M.; Sakakibara, K.; Komatsuzaki, T.; Akai, I. *Comp. Chem.* **1991**, *15*, 241–248.

(55) White, D.; Taverner, B. C.; Leach, P. G. L.; Coville, N. J. *J. Comput. Chem.* **1993**, *14*, 1042–1049.

(56) Taverner, B. C. *J. Comput. Chem.* **1996**, *17*, 1612–1623.

(57) Taverner, B. C., *STERIC, 1.11*, <http://www.ccl.net/cca/software/SOURCES/C/steric/index.shtml>, 1995.

(58) Peng, Q.; Yang, Y.; Wang, C.; Liao, X.; Yuan, Y. *Catal. Lett.* **2003**, *88*, 219–225.

(59) Gulyás, H.; Bényei, A. C.; Bakos, J. *Inorg. Chim. Acta* **2004**, *357*, 3094–3098.

(48) Becke, A. D. *J. Chem. Phys.* **1993**, *98*, 5648–5652.

(49) Lee, C.; Yang, W.; Parry, R. G. *Phys. Rev. B* **1988**, *37*, 785–789.

(50) Schäfer, A.; Horn, H.; Ahlrichs, R. *J. Chem. Phys.* **1992**, *97*, 2571–2577.

Table 4. Selected Geometrical Parameters for Calculated Pd⁰L Structures from DFT Calculations at the SVWN5/DGDZVP Level

complex	$R_{\text{Pd-P}}^a$ (Å)	$R_{\text{P-C}}^b$ (Å)	Pd-P-C ^c (deg)	C-P-C ^d (deg)	P-Pd-C-C ^e (deg)	$R_{\text{Pd-H}}^f$ (Å)	BDE ^g (kcal/mol)
Pd(TPPTS ³⁻)	2.149	1.823	111	108	-60	3.36	35.6
Pd(TPPTS·H ₃)	2.114	1.833	119	98	-46	3.29	36.5
Pd(TPPTS·Na ₃)	2.184	1.834	118	100	-62, -32, -14 ^h	3.25	37.7
Pd(TXPTS ³⁻)	2.182	1.817	110	109	-52	2.40	36.4
Pd(TXPTS·H ₃)	2.151	1.833	118	100	-39	2.35	31.9
Pd(TXPTS·H ₃) ⁱ	2.242	1.857	115	104	-45	2.56	42.1
Pd(TXPTS·Na ₃)	2.208	1.827	118	100	-50	2.51	36.5
Pd(TMAPTS ³⁻)	2.165	1.823	110	109	-53	2.60	35.7
Pd(TMAPTS·H ₃)	2.141	1.832	118	99	-47	2.44	33.0
Pd(TMAPTS·H ₃) ⁱ	2.159	1.817	114	105	-47	2.36	31.1
Pd(TMAPTS·Na ₃)	2.209	1.831	118	102, 98, 98 ^h	-57, -50, -39 ^h	2.52	35.0
Pd(PPh ₃)	2.132	1.824	116	102	-38	3.09	37.3
Pd(P(<i>o</i> -tol) ₃)	2.160	1.818	114	104	-48	2.36	32.0
Pd(TXP) ^j	2.163	1.816	114	105	-48	2.36	32.4
Pd(TMAP) ^k	2.166	1.820	114	105	-47	2.35	32.6
Pd(P(Mes) ₃) ^l	2.294	1.821	108	111	-45	2.13	26.3
Pd(P(2,4- <i>t</i> -Bu ₂ C ₆ H ₃) ₃)	2.268	1.842	115	103	-33	2.14	8.3

^a Pd-P bond distance. ^b Average P-C bond distance. ^c Average Pd-P-C bond angle. ^d Average C-P-C bond angle. ^e Average torsion angle between the Pd-P bond and the aryl ring plane. ^f Closest nonbonded Pd-H distances. ^g Bond dissociation energy ($E_{\text{Pd}} + E_{\text{L}} - E_{\text{PdL}}$). ^h Individual values for each aryl ring. ⁱ Non-hydrogen-bonded structure. ^j TXP = tri(2,4-dimethylphenyl)phosphine. ^k TMAP = tri(4-methoxy-2-methylphenyl)phosphine. ^l Mes = mesityl.

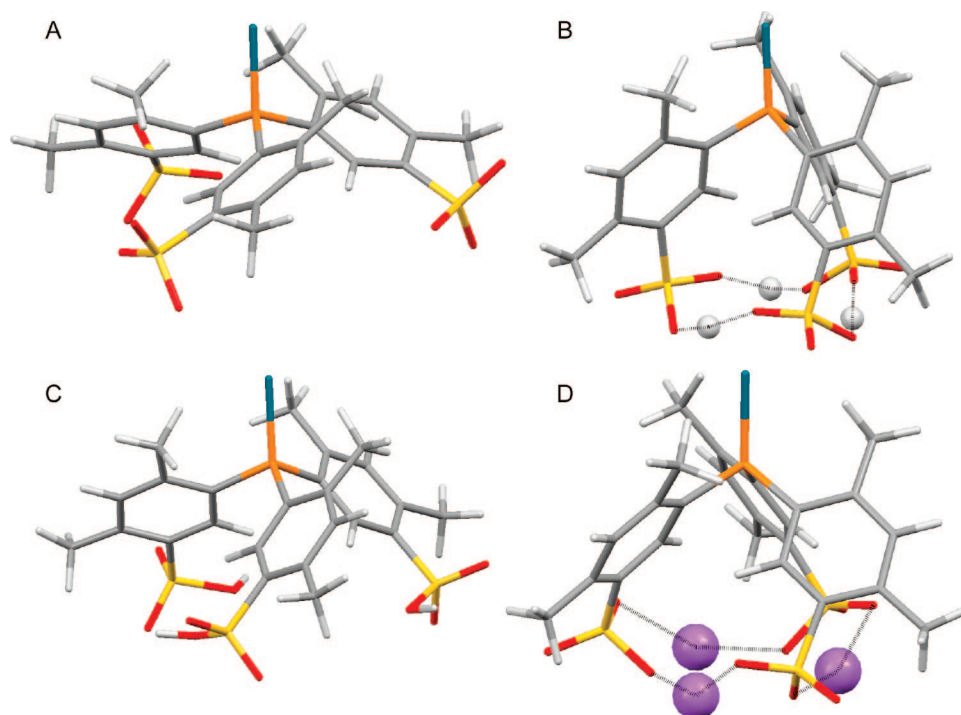


Figure 5. Cylindrical bond models of calculated Pd(TXPTS³⁻) (A), Pd(TXPTS·H₃) H-bonded (B), Pd(TXPTS·H₃) non-H-bonded (C), and Pd(TXPTS·Na₃) (D) structures. Carbon, gray; hydrogen, white; phosphorus, orange; sulfur, yellow; oxygen, red; palladium, blue; sodium, purple.

algorithm for calculating cone angles from solid angles has been reported by Tavener.⁵⁶ We have previously utilized Tavener's STERIC program,⁵⁷ which utilizes the solid angle algorithm, to calculate cone angle values based on DFT-optimized geometries of Pd-phosphine complexes.^{23,24} In contrast to Tolman's method, cone angles determined by this method have optimized Pd-P bond distances, and the phosphine substituents were allowed to adopt their most stable conformation, rather than the conformation leading to the smallest cone angle. The resulting cone angles should provide a more realistic picture of the true steric demand of ligands.

Cone angles (Table 5) for TPPTS, TXPTS, and TMAPTS were calculated from the LDA-optimized geometries for the Pd⁰(phosphine) complexes by using the STERIC program and the volumetric parameters for the atoms therein with the Pd

atom set at the origin.^{56,57} Previous estimates of the cone angle for TPPTS have ranged from 145° to 178°. Tolman's correlation between ³¹P NMR chemical shift and cone angle was used to estimate a value of 145° for TPPTS.³⁷ A low-level HF/3-21G* calculation of the cone angle predicted a value of 160°.⁵⁸ Cone angle values ranging from 152° to 178° have been determined on the basis of X-ray crystal structures of free TPPTS⁵⁹ and iron and tungsten carbonyl complexes.^{60,61} Our calculated value for TPPTS³⁻ is 155° (Table 5), while neutralization of the

(60) Darensbourg, D. J.; Bischoff, C. J.; Reibenspies, J. H. *Inorg. Chem.* **1991**, *30*, 1144-1147.

(61) Darensbourg, D. J.; Bischoff, C. J. *Inorg. Chem.* **1993**, *32*, 47-53.

(62) Pickett, T. E.; Roca, F. X.; Richards, C. J. *J. Org. Chem.* **2003**, *68*, 2592-2899.

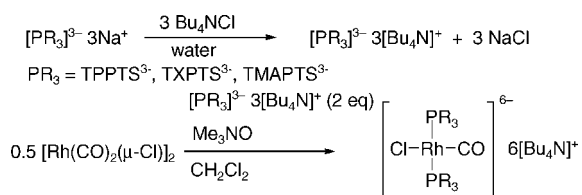
(63) Vastag, S.; Heil, B.; Markó, L. *J. Mol. Catal.* **1979**, *5*, 189-195.

Table 5. Experimental and Calculated Steric and Electronic Parameters for TPPTS, TXPTS, TMAPTS, and Related Nonsulfonated Ligands

ligand	cone angle ^a (deg)	ν_{CO}^b (cm ⁻¹)	free ligand			PdL complex		
			$q(\text{P})^c$	HOMO ^d (eV)	GAP ^e (eV)	$q(\text{P})^c$	HOMO ^d (eV)	GAP ^e (eV)
TPPTS ³⁻	155		0.18	1.18	4.65	0.03	1.81	2.47
TPPTS·H ₃	164		0.32	-7.39	4.80	0.17	-6.01	3.37
TPPTS·Na ₃	165	1993	0.29	-6.94	4.96	0.18	-5.64	3.48
TXPTS ³⁻	210		0.12	1.41	4.74	-0.04	1.81	2.40
TXPTS·H ₃	219		0.25	-6.82	4.89	0.13	-5.50	3.37
TXPTS·H ₃ ^f	209		0.17	-6.62	5.45	0.07	-5.49	3.31
TXPTS·Na ₃	206	1993	0.24	-6.55	4.87	0.09	-5.33	3.33
TMAPTS ³⁻	194		0.12	1.26	4.76	-0.05	1.74	2.48
TMAPTS·H ₃	214		0.27	-6.86	4.78	0.12	-5.64	3.41
TMAPTS·H ₃ ^f	215		0.16	-6.61	4.83	0.02	-5.52	3.27
TMAPTS·Na ₃	208	1993	0.26	-6.33	4.78	0.13	-5.21	3.29
PPh ₃	172	1979	0.26	-5.96	5.11	0.15	-4.89	3.38
P(<i>o</i> -tol) ₃	214	1972 ^g	0.17	-5.85	5.02	0.03	-4.77	3.17
TXP ^h	215		0.17	-5.63	4.96	0.03	-4.62	3.14
TMAP ⁱ	215		0.16	-5.36	4.85	0.04	-4.53	3.09
P(Mes) ₃ ^j	230	1964 ^k	0.12	-5.24	4.45	0.02	-4.31	2.87
P(2,4- <i>t</i> -BuC ₆ H ₃) ₃	280		0.11	-5.60	4.89	0.11	-4.01	3.26

^a Cone angle values determined from LDFT-optimized Pd⁰L structures using the STERIC program.^{56,57} ^b Carbonyl stretching frequency measured in solution (CH₂Cl₂) of *in situ* prepared *trans*-Rh(L)₂(CO)Cl complex. Tetrabutylammonium salts of TPPTS, TXPTS, and TMAPTS were used. ^c Charge on phosphorus calculated at the DFT level with the B3LYP exchange–correlation functional at the LDA-optimized geometry. ^d HOMO energy at the B3LYP level. ^e GAP = $E(\text{HOMO}) - E(\text{LUMO})$. ^f Non-hydrogen-bonded structure. ^g Literature value.⁶² ^h TXP = tri(2,4-dimethylphenyl)phosphine. ⁱ TMAP = tri(4-methoxy-2-methylphenyl)phosphine. ^j Mes = mesityl. ^k Estimated from the Tolman parameter obtained with Ni(P(Mes)₃)(CO)₃⁵² using the correlation reported by Vastag and co-workers.⁶³

Scheme 1. Synthesis of Rh Complexes of Sulfonated Phosphines after Cation Exchange



sulfonate charge with a proton or sodium ion gave larger cone angle values of 164° and 165°, respectively. The larger values for TPPTS·Na₃ and TPPTS·H₃ compared to TPPTS³⁻ result from the smaller Pd–P–aryl ring torsion angles for the sodium ion and proton adducts. As the aryl ring rotates toward becoming parallel with the P–Pd bond, the *ortho*-proton moves closer to the Pd center (shorter Pd–H interaction), leading to an increase in the cone angle (Figure 3). Interestingly, the TPPTS·Na₃ and TPPTS·H₃ structures have nearly identical cone angles despite their Pd–P bonds differing by 0.07 Å. The effect of the shorter bond for the TPPTS·H₃ structure is likely compensated by it having a larger average torsional angle than the TPPTS·Na₃ structure. The values calculated for TPPTS are in the mid range of previously reported values.

As expected, addition of a methyl group to the *ortho*-position of the aryl ring significantly increases the steric demand of the phosphines. Bakos⁵⁹ has previously reported cone angle values of 196° and 210° for TXPTS based on the X-ray crystal structure of the triguanidinium salt. The cone angle of TXPTS³⁻ calculated using the STERIC program is 210°. Protonation increased the cone angle to 219° for the more stable H-bonded structure, whereas the addition of sodium ions decreases the cone angle to 206°. The increase in cone angle on protonation is consistent with the smallest CPC angle for this structure (Figure 5). The small decrease on adding three Na⁺ ions is consistent with the increase in the Pd–P bond length and the small change in the CPC angle.

The cone angle of TMAPTS³⁻ was calculated to be 194°, and the value increases to 208° for TMAPTS·Na₃ and 214° for TMAPTS·H₃. The smaller calculated cone angle for

TMAPTS³⁻ than that of TXPTS³⁻ is consistent with the much larger agostic Pd–H interaction in the TXPTS³⁻ complex (2.40 Å) as compared to the TMAPTS³⁻ complex (2.60 Å). The values within the TMAPTS³⁻ series are consistent with the variations in the Pd–P bond lengths and torsional angles. The TMAPTS·H₃ structure has a smaller torsional angle and a shorter Pd–P bond than the TMAPTS³⁻ structure, both of which should make the Pd center more sterically hindered. The TMAPTS·Na₃ complex also has a smaller average torsional angle than the TMAPTS³⁻ structure, but a slightly longer bond. Therefore, the increase in cone angle is less for the TMAPTS·Na₃ complex than for TMAPTS·H₃. The cone angles for the TXPTS and TMAPTS qualitatively correlate with the agostic Pd–H interactions, with the stronger interactions (short Pd–H) correlating with increased cone angles.

The electron-donating ability of the ligands was determined experimentally from the CO stretching frequency of *trans*-RhL₂(CO)Cl complexes generated from the sulfonated phosphine tri(tetrabutylammonium (TBA)) salts and [Rh(CO)₂(μ-Cl)]₂ in the presence of trimethylamine *N*-oxide (Scheme 1).⁶³ The TBA salts were used to allow the sulfonated ligands to dissolve in methylene chloride. The TPPTS·(TBA)₃ complex in methylene chloride gave a CO stretching frequency of 1993 cm⁻¹ (Table 5). This value is at higher frequency than previously reported values of 1973–1982 cm⁻¹ for solid samples of *trans*-Rh(TPPTS·Na₃)₂(CO)Cl dispersed in KBr.^{64–66} Higher frequency values ranging from 1990 to 1994 cm⁻¹ have been reported for this complex supported in Zn–Al layered double hydroxide materials,⁶⁶ which shows that the CO stretch is sensitive to the surrounding environment. The rhodium complexes derived from TXPTS·(TBA)₃ and TMAPTS·(TBA)₃ gave identical CO stretching frequencies to the TPPTS·(TBA)₃ complex (1993 cm⁻¹). Thus on the basis of this measurement, there is no electronic difference among the sulfonated ligands.

(64) Herrmann, W. A.; Kellner, J.; Riepl, H. *J. Organomet. Chem.* **1990**, *389*, 103–128.

(65) Serp, P.; Hernandez, M.; Richard, B.; Kalck, P. *Eur. J. Inorg. Chem.* **2001**, 2327–2336.

(66) Zhang, X.; Wei, M.; Pu, M.; Li, X.; Chen, H.; Evans, D. G.; Duan, X. *J. Solid State Chem.* **2005**, *178*, 2701–2708.

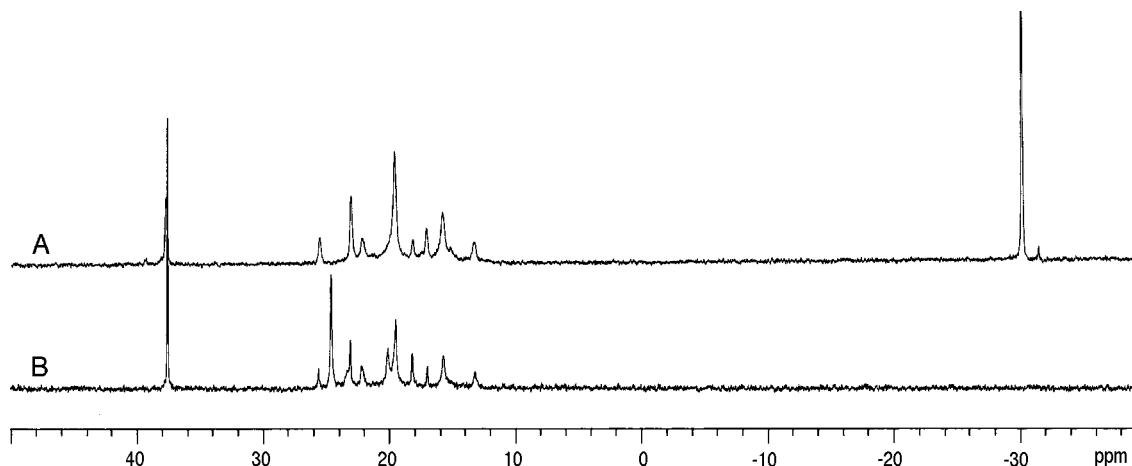


Figure 6. ^{31}P NMR spectra: (A) $\text{Pd}(\text{OAc})_2$ and TXPTS (2.4 equiv); (B) Na_2PdCl_4 and TXPTS (2.5 equiv).

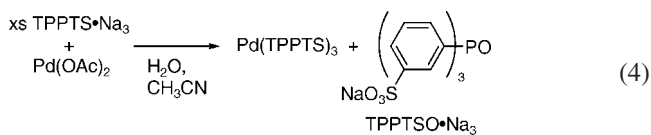
The sulfonated ligands are less electron donating than the analogous nonionic ligands (i.e., PPh_3 , TXP, and TMAP). Because of the range of CO stretching frequencies that have been reported for *trans*- $\text{Rh}(\text{TPPTS} \cdot \text{Na}_3)_2(\text{CO})\text{Cl}$, comparisons of sulfonated and nonsulfonated ligands must be made with some caution, however.

A variety of electronic properties—the charge on the P, the HOMO, and the GAP defined as $\text{GAP} = E(\text{HOMO}) - E(\text{LUMO})$ (Table 5)—were calculated for the sulfonated phosphines and their neutral analogues as both the free ligands and Pd-bound complexes. The charges on the P are all reduced on binding to Pd, with the exception of $\text{P}(2,4\text{-di-}t\text{-BuC}_6\text{H}_3)_3$, which did not change upon complexation probably due to the weak interaction of this ligand with Pd. If the counterions are not present, the charges on the P of the Pd complexes of the sulfonated ligands were near 0 or slightly negative. When the counterions are present, the charge on the P becomes substantially more positive. The charge on P for the $\text{TPPTS} \cdot \text{Na}_3$ and $\text{TPPTS} \cdot \text{H}_3$ complexes are the largest values, 0.18 and 0.17 e, respectively, even larger than the charge of 0.15 e on PPh_3 . The charges on the $\text{TMAPTS} \cdot \text{Na}_3$ and $\text{TMAPTS} \cdot \text{H}_3$ complexes are 0.13 and 0.12 e, respectively, both of which are slightly less than that on $\text{Pd}(\text{PPh}_3)$. The charge on P for the $\text{TXPTS} \cdot \text{Na}_3$ complex is 0.09 e, while the H-bonded $\text{TXPTS} \cdot \text{H}_3$ complex gave a similar value of 0.07 e. The less stable, non-H-bonded $\text{TXPTS} \cdot \text{H}_3$ and $\text{TMAPTS} \cdot \text{H}_3$ complexes had higher positive charges on P than the corresponding H-bonded structures. The lowest phosphorus charges (0.02–0.04 e) were seen for the *ortho*-methylated neutral phosphines ($\text{P}(o\text{-tol})_3$, TXP, TMAP, $\text{P}(\text{Mes})_3$). The sodium sulfonate and sulfonic acid groups increase the charge on P in all cases, but the effect is largest for the *ortho*-methylated ligands (i.e., TXP vs $\text{TXPTS} \cdot \text{Na}_3$).

The HOMO energy for the trianions is positive, as expected for a molecule with such a large negative charge. Addition of the counterions makes the HOMO energies negative. The HOMO energies of the neutral sulfonate complexes with the counterions present are the most negative. The lowest energy HOMO for the Na_3 complexes is that for $\text{TPPTS} \cdot \text{Na}_3$ followed by $\text{TXPTS} \cdot \text{Na}_3$ and $\text{TMAPTS} \cdot \text{Na}_3$. In the case of the sulfonic acids, $\text{Pd}(\text{TXPTS} \cdot \text{H}_3)$ has the highest energy HOMO followed by $\text{Pd}(\text{TMAPTS} \cdot \text{H}_3)$, while the $\text{TPPTS} \cdot \text{H}_3$ complex again had the lowest HOMO energy. PPh_3 has the lowest energy HOMO for nonsulfonated phosphines. Alkyl substituents tend to raise the HOMO energy, making the orbital more accessible. The GAPs for most of the compounds are in the range 3.1 to 3.5

eV except for $\text{P}(\text{Mes})_3$ with a GAP of 2.87 eV. The GAPs for the TPPTS , TXPTS , and TMAPTS complexes are in a narrow range between 3.3 and 3.5 eV.

Coordination Chemistry. Amatore and Jutand⁶⁷ have shown that TPPTS behaves in a similar manner to PPh_3 ^{68,69} when complexed to Pd^{II} salts in the presence of hard anions (OAc^- , OH^- , F^-). They observed that treatment of $\text{Pd}(\text{OAc})_2$ with an excess of $\text{TPPTS} \cdot \text{Na}_3$ in aqueous acetonitrile initially resulted in the formation of a Pd^{II} species, presumably $\text{Pd}(\text{TPPTS} \cdot \text{Na}_3)_2(\text{OAc})_2$. This Pd^{II} species underwent reductive elimination to give $\text{Pd}^0(\text{TPPTS} \cdot \text{Na}_3)_3$, or possibly $[\text{Pd}^0(\text{TPPTS} \cdot \text{Na}_3)_n(\text{OAc})]^-$,⁷⁰ and TPPTS -oxide ($\text{TPPTSO} \cdot \text{Na}_3$, eq 4). In order to compare the chemistry of TXPTS and TMAPTS with TPPTS , a series of studies were carried out to determine what complexes form from the combination of Pd^{II} salts and $\text{TXPTS} \cdot \text{Na}_3$ and $\text{TMAPTS} \cdot \text{Na}_3$ under conditions related to the catalytic reactions described above.



$\text{TXPTS} \cdot \text{Na}_3$ and Pd^{II} . A ^{31}P NMR spectrum of a solution of $\text{Pd}(\text{OAc})_2$ (0.1M) and $\text{TXPTS} \cdot \text{Na}_3$ (2.5 equiv) in 2:1 $\text{D}_2\text{O}/\text{acetonitrile}$ gave a peak for $\text{TXPTS} \cdot \text{Na}_3$ -oxide ($\text{TXPTSO} \cdot \text{Na}_3$) at 37.6 ppm; a complex set of peaks between 13 and 28 ppm, with the major resonance being at 19.5 ppm; and free $\text{TXPTS} \cdot \text{Na}_3$ at -30 ppm (Figure 6A). $\text{TXPTSO} \cdot \text{Na}_3$, which is present as an impurity (12 mol %) in the $\text{TXPTS} \cdot \text{Na}_3$ used in this work, serves as a convenient chemical shift and integration reference and is not expected to interact significantly with the palladium. The ratio of $\text{TXPTSO} \cdot \text{Na}_3$:13–28 ppm: $\text{TXPTS} \cdot \text{Na}_3$ was 7:71:22. The percentage of $\text{TXPTSO} \cdot \text{Na}_3$ present in this mixture is approximately the same as is present in the starting $\text{TXPTS} \cdot \text{Na}_3$, so no additional oxide appears to

(67) Amatore, C.; Blart, E.; Genêt, J. P.; Jutand, A.; Lemaire-Audoire, S.; Savignac, M. *J. Org. Chem.* **1995**, *60*, 829–839.

(68) Amatore, C.; Jutand, A.; M'Barki, M. A. *Organometallics* **1992**, *11*, 3009–3013.

(69) Amatore, C.; Carré, E.; Jutand, A.; M'Barki, M. A. *Organometallics* **1995**, *14*, 1818–1826.

(70) Amatore, C.; Carré, E.; Jutand, A.; M'Barki, M. A.; Meyer, G. *Organometallics* **1995**, *14*, 5605–5614.

(71) Baber, R. A.; Orpen, A. G.; Pringle, P. G.; Wilkinson, M. J.; Wingard, R. L. *Dalton Trans.* **2005**, 659–667.

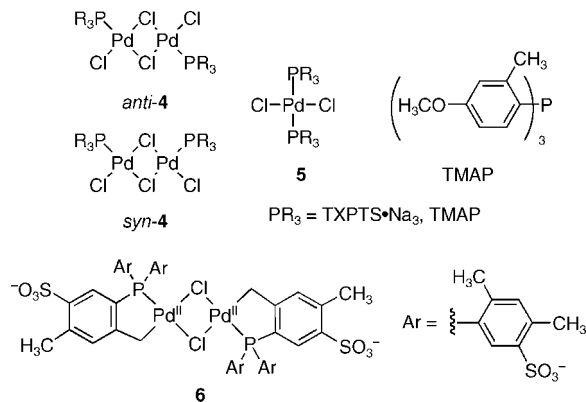


Figure 7. Proposed structures for TXPTS-coordinated palladium chloride complexes.

have formed. Treatment of this sample with phenyl iodide resulted in no change in any of the peak positions or intensities. Any Pd^0 species formed upon complexation with $\text{TXPTS} \cdot \text{Na}_3$ would be expected to oxidatively add phenyl iodide. The lack of reaction suggests that the cluster of peaks between 13 and 28 ppm represents various Pd^{II} complexes of $\text{TXPTS} \cdot \text{Na}_3$ and other ligands (^-OAc , ^-OH , H_2O , CH_3CN , etc.).

The complexation of $\text{TXPTS} \cdot \text{Na}_3$ with Na_2PdCl_4 in 2:1 D_2O /acetonitrile was next explored. Using a 2.5:1 $\text{TXPTS} \cdot \text{Na}_3/\text{Na}_2\text{PdCl}_4$ ratio, a similar pattern of peaks was observed between 13 and 28 ppm to that seen in the $\text{Pd}(\text{OAc})_2$ reaction was observed (Figure 6B, $\text{TXPTS} \cdot \text{Na}_3:\text{Pd}^{\text{II}}:\text{TXPTS} \cdot \text{Na}_3 = 14:86:0$). All of the peaks from the $\text{Pd}(\text{OAc})_2$ reaction were present in similar relative ratios. In addition, two new resonances at 24.6 and 20.1 ppm were observed, which were not present when $\text{Pd}(\text{OAc})_2$ was used as the Pd precursor. Presumably these new peaks represent chloride complexes. The other difference relative to the $\text{Pd}(\text{OAc})_2$ studies was that no free $\text{TXPTS} \cdot \text{Na}_3$ was present in the sample. When the amount of $\text{TXPTS} \cdot \text{Na}_3$ was increased to 5 equiv relative to Pd, the ^{31}P NMR spectrum showed $\text{TXPTS} \cdot \text{Na}_3$, a cluster of peaks between 13 and 28 ppm, and free $\text{TXPTS} \cdot \text{Na}_3$ (15:53:34). Neither the 24.6 nor 20.1 ppm resonances were observed, but a new peak was observed at 18 ppm. Other than the addition of the peak at 18 ppm, the pattern was identical to that seen when $\text{Pd}(\text{OAc})_2$ was used as the Pd source.

We have tentatively assigned the resonances at 24.6 and 20.1 ppm to *anti*- and *syn*- $[\text{Pd}(\text{TXPTS})(\mu\text{-Cl})\text{Cl}]_2$ (**4**, Figure 7). The fact that these resonances disappear when additional ligand is added suggests that they correspond to monophosphine complexes. Orpen and Pringle⁷¹ have reported the synthesis of a structurally similar $[\text{PdL}(\mu\text{-Cl})\text{Cl}]_2$ complex ($\text{L} = \text{tri}(4\text{-methoxy-2-methylphenyl})\text{phosphine}$ (TMAP)). The ^{31}P NMR chemical shifts for the *syn*- and *anti*-isomers of this complex were found at 24.1 and 22.4 ppm in CD_2Cl_2 . Another possible structure that could be considered is the palladacycle μ -chloride dimer (**6**). This possibility appears less likely, since the related palladacycles derived from TMAP and $\text{P}(o\text{-tol})_3$ have chemical shifts of 29 and 39 ppm, respectively.^{72,73} The peak observed at 18 ppm has been assigned to $\text{Pd}(\text{TXPTS})_2\text{Cl}_2$ (**5**), since this resonance was only observed at high TXPTS/Pd ratios and in the presence of chloride. In addition, Orpen and Pringle reported a chemical shift of 18.8 ppm for *trans*- $\text{Pd}(\text{TMAP})_2\text{Cl}_2$.

The remaining peaks observed between 13 and 28 ppm cannot have acetate or chloride coordinated, as they have been observed in approximately the same relative intensities when using $\text{Pd}(\text{OAc})_2$ or Na_2PdCl_4 as the palladium source (Figure 6). Therefore, these species must have only TXPTS, water, hydroxide, and acetonitrile as ligands. In addition, the sulfonate groups of the ligands could bind in a κO fashion in addition to the expected κP binding. The two most intense features in this region are the peak at 19.5 ppm and an AB doublet pair at 24.3 and 14.5 ppm ($^2J_{\text{P,P}} = 506$ Hz). We propose that the 19.5 ppm resonance and the other minor peaks at 22.2, 18.2, and 17.0 ppm are $\text{Pd}(\text{TXPTS})_n\text{L}_m$ complexes (**7**, $n = 1, 2$; $m = 0\text{--}3$; $\text{L} = \text{water, hydroxide, acetonitrile}$). Possible structures for complex **7** are listed in Figure 8.

The peak splitting in the AB doublet pattern remained constant when the NMR operating frequency was changed from 145.8 to 202.5 MHz, which supports the conclusion that these peaks are truly coupled. The large coupling constant is consistent with a 2J coupling between chemically unique phosphorus nuclei in a *trans*-relationship. Since TXPTS is the only phosphine present initially, some of the TXPTS must be modified in the course of the reaction, which would most likely occur by activation of a C–H bond of one of the *o*-methyl groups to form a palladacycle.⁷⁴ Palladium complexes of (*o*-methylphenyl)phosphines (i.e., tri(*o*-tolyl)phosphine) are known to form palladacyclic complexes of this type under mild conditions.^{72,73,75,76} In addition, our DFT-optimized structures showed close contacts between hydrogens on the *ortho*-methyl groups and palladium. Therefore, the AB pattern has been tentatively assigned to $[\text{Pd}(\kappa^2\text{C},\text{P-TXPTS})(\kappa\text{P-TXPTS})\text{L}]$ (**8**, Figure 9, $\text{L} = \text{water, hydroxide, acetonitrile, or no ligand}$). In a structurally related palladacycle derived from trimesitylphosphine (**9**, $\text{X} = \text{Cl, Br, I}$), the reported chemical shifts of the metalated phosphine ranged from 22.1 to 22.5 ppm and the $^2J_{\text{P,P}}$ values ranged from 414 to 419 Hz.⁷⁷

TXPTS \cdot Na₃, Pd(OAc)₂, and Na₂CO₃. Since base is present in all of the coupling reactions, a mixture of $\text{Pd}(\text{OAc})_2$ (0.2 M), $\text{TXPTS} \cdot \text{Na}_3$ (2.7 equiv), and sodium carbonate (6.6 equiv) in 2:1 D_2O /acetonitrile was analyzed by ^{31}P NMR spectroscopy. Immediately after mixing, only three resonances were seen in the ^{31}P NMR spectrum: $\text{TXPTS} \cdot \text{Na}_3$, a peak at 19.5 ppm (**7**), and free $\text{TXPTS} \cdot \text{Na}_3$ in a 12:38:50 ratio. After standing for 48 h, the peaks present were $\text{TXPTS} \cdot \text{Na}_3$, a new peak at 20.1 ppm, **7**, and free $\text{TXPTS} \cdot \text{Na}_3$ in a 14:7:24:55 ratio. $\text{TXPTS} \cdot \text{Na}_3$ comprised 14% of the total area, so little additional $\text{TXPTS} \cdot \text{Na}_3$ had been formed under these conditions. The new peak at 20.1 ppm appears to have been formed from **7**, since the peak at 19.5 ppm had decreased in intensity from the initial spectrum. Addition of phenyl iodide again had no effect on this mixture. Therefore, the peak at 20.1 ppm does not correspond to a Pd^0 complex. Since this species is only seen when carbonate is present, it has tentatively been assigned as $[\text{Pd}(\text{TXPTS})_n(\text{CO}_3)]\text{Na}_{3n}$ (eq 5, **10**). The presence of carbonate decreased the amount of $\text{TXPTS} \cdot \text{Na}_3$ bound to palladium. In the absence of sodium carbonate, 76% of the $\text{TXPTS} \cdot \text{Na}_3$ ($\text{TXPTS} \cdot \text{Na}_3:\text{Pd}(\text{OAc})_2 = 2.5$) was bound to Pd^{II} , while 24%

(74) While $\text{TXPTS} \cdot \text{Na}_3$ could potentially coordinate to Pd, the 3J coupling would be expected to be much smaller than is observed.

(75) Cheney, A. J.; Shaw, B. L. *J. Chem. Soc., Dalton Trans.* **1972**, 860–865.

(76) Herrmann, W. A.; Brossmer, C.; Öfele, K.; Reisinger, C.-P.; Priemeier, T.; Beller, M.; Fischer, H. *Angew. Chem., Int. Ed.* **1995**, *34*, 1844–1848.

(77) Alyea, E. C.; Malito, G. *Gazz. Chim. Ital.* **1993**, *123*, 709–711.

(72) Alyea, E. C.; Malito, J. *J. Organomet. Chem.* **1988**, *340*, 119–126.

(73) Herrmann, W. A.; Brossmer, C.; Reisinger, C.-P.; Riermeier, T. H.; Öfele, K.; Beller, M. *Chem.–Eur. J.* **1997**, *3*, 1357–1364.

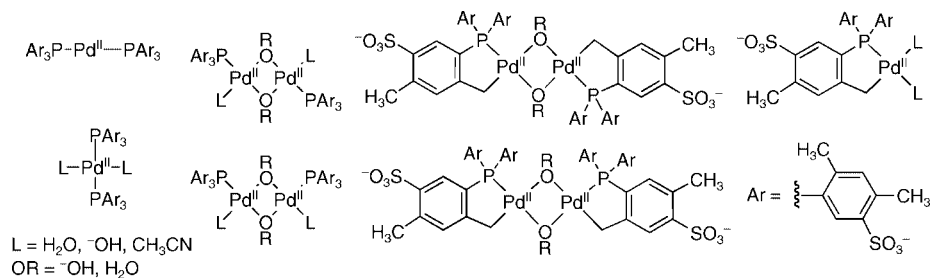


Figure 8. Possible structures for complexes observed between 13 and 28 ppm (**7**).

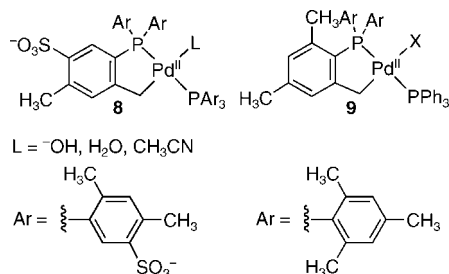
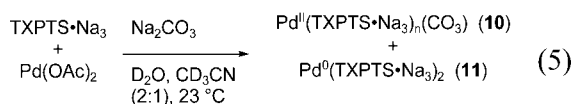


Figure 9. Proposed palladacycle structure for the AB quartet feature.

was uncoordinated. In the presence of 6.5 equiv of sodium carbonate, only 43% of the ligand was coordinated to Pd^{II}.



The ratio of carbonate to Pd is much higher under catalytic conditions, so the complexation reaction was repeated in the presence of 27 equiv of sodium carbonate (Pd/TXPTS·Na₃ 2.5:1). Under these conditions, TXPTS·Na₃, the resonance at 19.5 ppm (**7**), and free TXPTS·Na₃ remained the major resonances observed immediately after mixing. The peak at 19.5 ppm was much broader than when a lower amount of carbonate was used, suggesting a possible equilibrium between **7** and a carbonate-bound complex (**10**). In addition, a small peak at -9.6 ppm was observed (TXPTS·Na₃: -9.6 ppm:TXPTS·Na₃ = 18:27:7:47). The amount of TXPTS·Na₃ was larger than is present in the starting TXPTS·Na₃ (12%), showing that some additional TXPTS·Na₃ had formed under these conditions. After standing for a day, the same peaks were present with the exception of **7**, which had been replaced by complex **10** (20.1 ppm). The TXPTS·Na₃:**10**: -9.6:TXPTS·Na₃ ratio was 29:29:15:27. Thus the amount of TXPTS·Na₃ and the -9.6 ppm peak had increased at the expense of the decrease of the amount of TXPTS·Na₃. The new peak at 20.1 was nearly identical in size to that of **7** seen in the initial spectrum.

Addition of phenyl iodide to this mixture resulted in the immediate loss of the peak at -9.6 ppm, indicating that this species is a Pd⁰ complex of TXPTS·Na₃. The free TXPTS·Na₃ peak increased in intensity to 61% of the total integrated value after the phenyl iodide was added. In addition to TXPTS·Na₃ (17%), the only other peak present was a broad peak centered at 20 ppm (22%). On the basis of the similar chemical shift of bis(tri(2,4-dimethylphenyl)phosphine)palladium(0) (Pd(TXP)₂, -8.5 ppm),⁷⁸ the -9.6 resonance has been tentatively assigned to Pd⁰(TXPTS·Na₃)₂ (**11**). The formation of **11** could be

accelerated by heating the reaction mixture at 50 °C. After heating the reaction for 2.5 h at 50 °C, **11** was the major species present in solution along with smaller amounts of TXTPSO·Na₃ and free TXPTS·Na₃ (TXTPSO·Na₃:**11**:TXPTS·Na₃ = 12:76:12).

TXPTS·Na₃, Pd(OAc)₂, PhB(OH)₂, and Na₂CO₃. The other component present in the Suzuki coupling is phenylboronic acid, which can reduce Pd^{II} in the presence of base or oxyanion ligands (-OAc, -OH) by transferring two phenyl groups to the Pd^{II} complex followed by reductive elimination of biphenyl.^{23,79} A solution of Pd(OAc)₂, TXPTS·Na₃ (2.4 equiv), Na₂CO₃ (6.6 equiv), and PhB(OH)₂ (16.4 equiv) in 2:1 D₂O/acetonitrile was analyzed by ³¹P NMR spectroscopy immediately after mixing. The major species present were TXTPSO·Na₃ (14%), **7** (18%), and free TXPTS·Na₃ (68%). No Pd⁰(TXPTS)₂ (**11**) was present initially. After standing for 24 h at room temperature, complex **7** had been replaced by **11** (TXTPSO·Na₃:**11**:TXPTS·Na₃ = 19:22:59). Complex **7** appears to have been converted to the Pd⁰ complex, while there were no significant changes in the amounts of TXTPSO·Na₃ and TXPTS·Na₃. Treatment of this solution with phenyl iodide resulted in the complete loss of **11**, the formation of **7**, and an AB pattern at 21.1 and 15.1 ppm with a coupling constant of 363 Hz, along with some additional minor peaks between 14 and 28 ppm (TXTPSO·Na₃:**7**:AB pattern:TXPTS·Na₃ = 18:7:19:41).

When the amount of base was increased significantly (TXPTS·Na₃ (2.8 equiv), Na₂CO₃ (103 equiv), PhB(OH)₂ (3.9 equiv)), there was only a small amount of **7** present (4% of total integrated area) immediately after the components were combined. A significant amount of Pd⁰(TXPTS)₂ (**11**) had already formed (20%) after a few minutes. Free TXPTS·Na₃ (61%) and TXTPSO·Na₃ (15%) comprised the remainder of the material. Since little additional TXTPSO·Na₃ had formed, PhB(OH)₂ appears to be the reductant under these conditions. After standing for 24 h at room temperature, only TXTPSO·Na₃ (18%), **11** (62%), and TXPTS·Na₃ (20%) were present.

The ¹H NMR spectrum of this mixture showed two broad resonances in the aromatic region due to TXPTS·Na₃ that were shifted upfield from those of free TXPTS·Na₃. The phenylboronic acid resonances were also shifted upfield, presumably due to the formation of PhB(OH)₃⁻ under the strongly basic reaction conditions. The alkyl region showed a small amount of TXTPSO·Na₃ and two resonances that presumably correspond to the Pd⁰ complex. A peak was observed in the same position as the *para*-methyl of free TXPTS (2.48 ppm).⁸⁰ Another broad resonance was observed at 2.60 ppm, which may correspond to the *ortho*-methyl groups of the Pd⁰ complex. This resonance was downfield of where the *ortho*-methyl of free TXPTS·Na₃ was observed (2.24 ppm).

(79) Adamo, C.; Amatore, C.; Ciofini, I.; Jutand, A.; Lakmini, H. *J. Am. Chem. Soc.* **2006**, *128*, 6829–6836.

(80) ¹H and ¹³C resonances were fully assigned based on HSQC/HMBC spectra. See Supporting Information for a full description.

(78) Paul, F.; Patt, J.; Hartwig, J. F. *Organometallics* **1995**, *14*, 3030–3039.

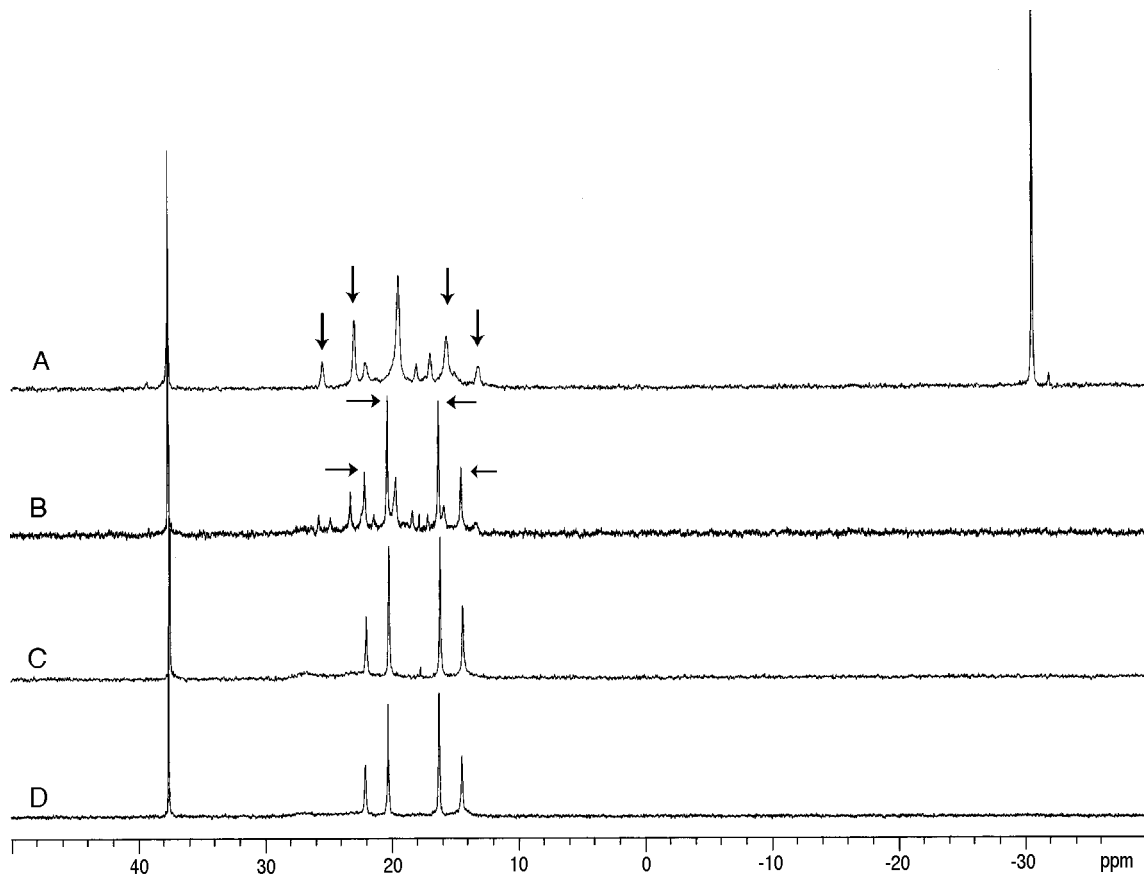


Figure 10. ^{31}P NMR spectra of Pd/TXPTS \cdot Na $_3$: (A) Pd(OAc) $_2$ and TXPTS \cdot Na $_3$ (2.4 equiv), arrows indicate the AB quartet feature; and Pd(OAc) $_2$, TXPTS \cdot Na $_3$ (2.5 equiv), and PhB(OH) $_2$ (4.0 equiv): (B) after 1 h, arrows indicate the new AB quartet; (C) after 24 h; (D) after 5 days.

Although a significant amount of **11** could be generated in the presence of phenylboronic acid and a large excess of base, the rate was still slow compared to the catalytic reactions. The catalytic reactions were all performed at 50 °C, or higher, however. When the complexation of TXPTS \cdot Na $_3$ (4:1 TXPTS \cdot Na $_3$ /Pd) with Pd(OAc) $_2$ in the presence of Na $_2$ CO $_3$ (20 equiv) and PhB(OH) $_2$ (10 equiv) was performed at 50 °C, the Pd 0 (TXPTS) $_2$ (**11**) species was the major species after a period of 3 h (TXPTS \cdot Na $_3$:**11**:TXPTS \cdot Na $_3$ = 12:76:12).

TXPTS \cdot Na $_3$, Pd(OAc) $_2$, and PhB(OH) $_2$. Reaction of TXPTS \cdot Na $_3$ (2.5 equiv), Pd(OAc) $_2$, and PhB(OH) $_2$ (4 equiv) in 2:1 D $_2$ O/CD $_3$ CN in the absence of sodium carbonate gave a complex mixture of Pd $^{\text{II}}$ species between 14 and 26 ppm (Figure 10), while no free TXPTS \cdot Na $_3$ was observed. The cluster of peaks between 14 and 26 ppm contained **7**, palladacycle **8**, and the other minor species that were also observed in the absence of PhB(OH) $_2$ (Figure 6). The major species present in this region was a new AB pair of doublets with chemical shifts of 21.1 and 15.1 ppm and a coupling constant of 363 Hz. The spectral data for the AB doublet pair were identical to one of the species formed when **11** was treated with phenyl iodide. After standing for 24 h at room temperature, the AB pattern was the major phosphorus-containing species present in solution other than TXPTS \cdot Na $_3$. In addition, some very broad resonances were observed between 20 and 30 ppm.

At room temperature, the aromatic region of the ^1H NMR spectrum of the reaction mixture containing the AB pattern and TXPTS \cdot Na $_3$ showed only phenylboronic acid and a small amount of TXPTS \cdot Na $_3$. No resonances corresponding to the

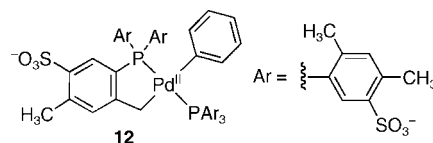
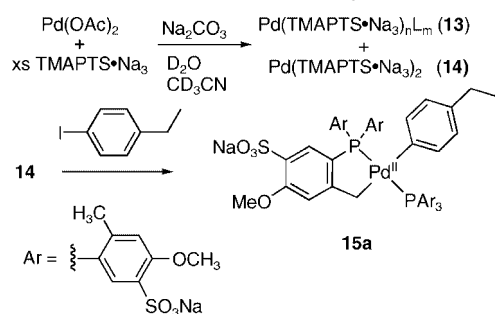


Figure 11. Proposed structure of the palladacycle formed in the presence of PhB(OH) $_2$.

AB pattern were observed. The alkyl region of this mixture showed TXPTS \cdot Na $_3$ and a trace of free TXPTS \cdot Na $_3$. Several very broad resonances in the baseline were observed that presumably correspond to the complex responsible for the AB doublet pair. Thus it appears that the TXPTS ligands are undergoing a dynamic process on the ^1H NMR time scale, resulting in very broad resonances. ^1H NMR spectra obtained at various operating frequencies (360–600 MHz) and over the temperature range accessible in the solvent system also gave broad unresolved peaks that did not allow the structure of the complex to be conclusively determined.

The complex with the 363 Hz coupling has been observed upon the reaction of phenyl iodide with **11** and when TXPTS \cdot Na $_3$ is reacted with Pd(OAc) $_2$ in the presence of phenylboronic acid. We propose that this complex is an analogue of **8** where L = phenyl-[Pd(κ^2 C,*P*-TXPTS \cdot Na $_3$)(κ *P*-TXPTS \cdot Na $_3$)Ph] (Figure 11, **12**). Introduction of the phenyl substituent is consistent with the conditions under which **12** is generated, as well as the smaller $^2J_{\text{P,P}}$ value for **12** compared to **8**. Replacement of a weak *cis*-influence ligand (^-OH , H $_2$ O, or CH $_3$ CN) in **8** with phenyl would be expected to decrease the

Scheme 2. Reaction of TMAPTS·Na₃ with Pd(OAc)₂ in the Presence of Na₂CO₃


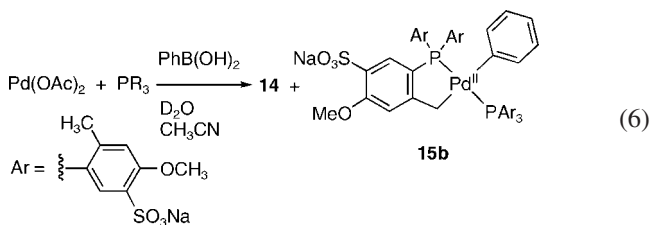
²J_{P,P} value due to phenyl's larger *cis* influence. Unfortunately the ambiguous nature of the ¹H and ¹³C NMR spectra of this complex and our inability to isolate X-ray quality crystals of it do not allow us to unambiguously assign the structure of **12**.

TMAPTS·Na₃ Complexation with Pd(OAc)₂. The complexation of TMAPTS·Na₃ with Pd(OAc)₂ was also explored. Analysis of a solution comprised of Pd(OAc)₂, TMAPTS·Na₃ (3.5 equiv), and sodium carbonate (20 equiv) in 2:1 water/acetonitrile by ³¹P NMR spectroscopy gave resonances at 37.3 (TMAPTS-oxide (TMAPTSO·Na₃), 19.3 (broad), and -11.2 ppm (integrated ratio: 30:23:47) immediately after mixing the reagents. No free TMAPTS·Na₃ was observed under these conditions. The TMAPTS·Na₃ used in these studies had only a trace of TMAPTSO·Na₃ present, so all of the oxide formed is a result of the reduction of Pd^{II}. No change was observed in spectra of the reaction mixture over a period of 2 h, other than a slight increase in the amount of the TMAPTSO·Na₃ peak relative to the -11.2 ppm peak (36:22:42 after 2 h). 4-Ethyl iodobenzene was added to this mixture. Immediately after adding the aryl iodide, the -11.2 ppm peak was nearly completely consumed. The peak at 19.3 ppm remained and a new pair of doublets at 19.1 and 13.4 ppm (²J_{P,P} = 376 Hz) appeared in the spectrum.

The 19.3 ppm resonance is presumably due to a similar Pd^{II}(TMAPTS·Na₃)_nL_m (L = acetonitrile, hydroxide, or water) species to **7** (Scheme 2, **13**). The -11.2 ppm peak disappears in the presence of an aryl iodide, so it is likely Pd⁰(TMAPTS·Na₃)₂ (**14**), in analogy to **11**, which was observed at -9.6 ppm in the TXPTS system. The pair of doublets feature that formed when the Pd⁰ complex reacted with the aryl iodide has similar chemical shift and coupling constant values to **12**. In analogy to **12**, the AB pattern has been assigned to a palladacycle complex ([Pd(κ²C,P-TMAPTS)(κP-TMAPTS)Ar] Na₆, Ar = 4-ethylphenyl, **15a**). This complex is formed by a sequence of events involving oxidative addition of the aryl iodide and C-H activation of an *ortho*-methyl group on the ligand.

A solution of Pd(OAc)₂, TMAPTS·Na₃ (3.5 equiv), sodium carbonate (20 equiv), and phenylboronic acid (10 equiv) was then analyzed by ³¹P NMR spectroscopy (eq 6). Only a trace of TMAPTSO·Na₃ was observed. A similar set of AB doublets was present, which presumably belongs to the Ph analogue of **15a** (eq 3, **15b**), along with Pd⁰(TMAPTS)₂ (**14**) and free TMAPTS·Na₃ (-35.5 ppm, broad) (36:47:17 integrated ratio). This system remained unchanged over the course of 2 h. Upon addition of 4-ethyl iodobenzene, the amount of **14** decreased, while resonances for **15** and the TMAPTS·Na₃ peak became more intense (**15**:**14**:TMAPTS·Na₃ = 42:36:21). Upon standing, complex **14** continued to slowly decay, while the amount of free TMAPTS·Na₃ slowly increased. After standing for 3 h, the ratio had changed to 41:30:29. The loss of **14** is much slower

than in the previous case, because this is a complete catalytic system in which **14** can be continually regenerated.



Calculated ³¹P NMR Chemical Shifts. Since we were unable to isolate pure palladium complexes of sulfonated ligands, the ³¹P NMR chemical shifts were calculated for the compounds with the pure DFT gradient-corrected BLYP exchange-correlation functional⁸¹ and the TZP basis set using the ADF code.^{82,83} The NMR calculations were done in the gauge invariant atomic orbital (GIAO) approach at the DFT level based on the developments in the Ziegler group.⁸⁴⁻⁸⁷ Scalar relativistic effects were included at the two-component zero-order regular approximation (ZORA) level for the NMR calculations (inclusion of the mass-velocity and Darwin terms).⁸⁷⁻⁸⁹ The standard for the calculations is H₃PO₄ with an absolute chemical shift of 292.2 ppm. We first compare the calculated and experimental value for PPh₃. The isolated molecule value is 9.4 ppm, 15 ppm larger than experiment. Variation of the Pd-P-C-C torsion angle by +10° leads to a value of 0.6 ppm, differing by 6 ppm from experiment. Placing PPh₃ in a self-consistent reaction field⁹⁰ with the COSMO parameters⁹¹⁻⁹³ and with a value for the dielectric of DMF leads to only a slight decrease in the chemical shift to 8.1 ppm. Thus the variation in the torsion angle is more important in determining the chemical shift than the surrounding medium. For Pd(PPh₃)₂, the agreement between the calculated and experimental values is within ~2 ppm. Similar good agreement is found for Pd(P(*t*-Bu)₃)₂ and P(*t*-Bu)₃. Inclusion of solvent effects, in this case THF at the COSMO level, leads to slightly worse agreement with experiment (calculated value = 67.9 ppm). The calculated value for TXPTS³⁻ differs by almost 50 ppm from the experimental value. When the ³¹P chemical shifts for the sulfonic acid or trisodium salt derivatives were calculated, much better agreement with experiment was found, with the sodium salt providing the closest agreement. The calculated value for **11** differs by only 14 ppm from experiment even though no counterions are present.

(81) Becke, A. D. *Phys. Rev. A* **1988**, *38*, 3098-3100.

(82) See also: *ADF 2004.01*; ADF Users Guide, <http://www.scm.com>, SCM, Theoretical Chemistry, Vrije Universiteit, Amsterdam.

(83) te Velde, G.; Bickelhaupt, F. M.; Baerends, E. J.; Fonseca Guerra, C.; van Gisbergen, J. A.; Snijders, J. G.; Ziegler, T. *J. Comput. Chem.* **2001**, *22*, 931-967.

(84) Schreckenbach, G.; Ziegler, T. *J. Phys. Chem.* **1995**, *99*, 606-611.

(85) Schreckenbach, G.; Ziegler, T. *Int. J. Quantum Chem.* **1997**, *61*, 899-918.

(86) Wolff, S. K.; Ziegler, T. *J. Chem. Phys.* **1998**, *109*, 95-905.

(87) Wolff, S. K.; Ziegler, T.; van Lenthe, E.; Baerends, E. J. *J. Chem. Phys.* **1999**, *110*, 7689-7698.

(88) van Lenthe, E.; Baerends, E. J.; Snijders, J. G. *J. Chem. Phys.* **1993**, *99*, 4597-4610.

(89) Autschbach, J.; Ziegler, T. In *Calculation of NMR and EPR Parameters: Theory and Application*; Kaupp, M., Buhl, M., Malkin, V. G., Eds.; Wiley-VCH & Co.: Weinheim, 2004; pp 249-264.

(90) Tomasi, J.; Mennucci, B.; Cammi, R. *Chem. Rev.* **2005**, *105*, 2999-3093.

(91) Klamt, A. *J. Phys. Chem.* **1995**, *99*, 224-2235.

(92) Klamt, A.; Schüürmann, G. *J. Chem. Soc., Perkin Trans. 2* **1993**, 799-805.

(93) Klamt, A.; Jonas, V. *J. Chem. Phys.* **1996**, *105*, 9972-9981.

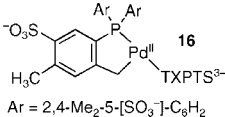
The calculated chemical shifts for the Pd(κ^2C,P -TXPTS)(κP -TXPTS) complex (**16**) without counterions were predicted to be 40.3 and 47.9 ppm, which are 25 to 30 ppm higher than either of the proposed palladacycle complexes (**8** and **12**). The inclusion of Na⁺ counterions did not substantially improve the agreement. It is possible that a fourth ligand is coordinated to the Pd center, which would affect the chemical shift, although steric hindrance may preclude the presence of an additional ligand. GIAO⁹⁴ calculations of the chemical shift with the B3LYP functional and the Ahlrichs triple- ζ basis set⁵⁰ gave predicted chemical shifts of 16.0 and 22.7 ppm, which are in excellent agreement with the observed values for **8** and **12**. However, the agreement between the B3LYP calculations and experiment for the ³¹P chemical shifts for the other compounds in Table 6 was generally not as good as that from the GIAO/ZORA calculations. Overall, the calculations provide estimates of the ³¹P chemical shifts for these types of complexes that are only accurate to within about 15 ppm, which are insufficient to reach any conclusions regarding the proposed structure assignments.

Discussion

Ligand Structure, Steric, and Electronic Properties. The presence or absence of a counterion and the identity of the ion were found to have a significant effect on the calculated structure and cone angle of the sulfonated ligands. Predicted structures without counterions for the sulfonate groups resulted in structures adopting an open conformation typified by smaller Pd–P–C angles, larger C–P–C angles, and larger Pd–P–C–C torsion angles. As a result, the sulfonate ions were able to achieve maximum separation, thus reducing the charge repulsion. When sodium ions or protons were added to the sulfonate groups, the geometry of the ligand changed to bring the sulfonate groups closer together. In the L·Na₃ structures, each sodium ion was coordinated to two sulfonate groups, while in the case of the L·H₃ structures hydrogen bonding occurred between the sulfonate groups. In order to allow the proton or sodium ion to interact with more than one sulfonate group, the aryl rings were pulled back from the Pd center (larger Pd–P–C and smaller C–P–C angles) and the torsional angle was decreased for some of the aryl rings. The result of these conformation changes was an increase in cone angle by 10–20° from the L³⁻ structure to the L·Na₃ and L·H₃ structures. In the cases where a hydrogen-bonded structure could be compared to a non-hydrogen-bonded structure (TXPTS and TMAPTS), the former was always more stable than the latter for both the free ligand and the palladium complex. The results suggest that solvent and counterions can play a role in determining the actual value of the cone angles.

The calculated cone angle values show the importance of carefully considering the structural model to use when ionic groups are present on the ligand. For the trianionic structures, the cone angle trend is TPPTS³⁻ << TMAPTS³⁻ << TXPTS³⁻; the sodium salts follow the trend TPPTS·Na₃ << TXPTS·Na₃ ≈ TMAPTS·Na₃; and for the sulfonic acid structures the trend is TPPTS·H₃ << TMAPTS·H₃ < TXPTS·H₃. In all three cases, the *ortho*-methylated structures have much larger cone angles than TPPTS, but what do these

Table 6. Calculated and Experimental ³¹P NMR Chemical Shifts

species	exp. δ (ppm) ^a	GIAO/ ZORA calc. δ (ppm) ^b	B3LYP/ Ahlrichs calc. δ (ppm) ^c
PPh ₃	-5.4 ^c	9.4	-13.0
Pd(PPh ₃)		79.4	48.4
Pd(PPh ₃) ₂	31.0 ^d	29.3	10.7
Pd(P(<i>o</i> -tol) ₃)		12.4	
Pd(TXP)		12.4	
Pd(TMAP)		12.4	
Pd(P(Mes) ₃)		-25.5	
Pd(P(2,4- <i>t</i> -BuC ₆ H ₃) ₃)		-24.9	
P(<i>t</i> -Bu) ₃	63.4 ^e	65.5	51.1
Pd(P(<i>t</i> -Bu) ₃) ₂	85.6 ^e	84.3	72.4
TPPTS ³⁻		30.9	
TPPTS·H ₃		-8.0	
TPPTS·Na ₃	-5	-3.0	
Pd(TPPTS ³⁻)		89.7	
Pd(TPPTS·H ₃)		54.5	
Pd(TPPTS·Na ₃)		59.7	
TXPTS ³⁻		20.3	-1.4
TXPTS·H ₃		-43.7	
TXPTS·H ₃ ^g		-10.4	
TXPTS·Na ₃	-31.4	-32.2	
Pd(TXPTS ³⁻)		45.5	12
Pd(TXPTS·H ₃)		-26.3	
Pd(TXPTS·H ₃) ^g		21.7	
Pd(TXPTS·Na ₃)		-11.1	
Pd(TXPTS ³⁻) ₂ (11)	-9.6	4.3	-16.3
TMAPTS ³⁻		21.2	
TMAPTS·H ₃		-32.9	
TMAPTS·H ₃ ^g		-11.9	
TMAPTS·Na ₃	-29.5	-28.8	
Pd(TMAPTS ³⁻)		60.8	
Pd(TMAPTS·H ₃)		-14.1	
Pd(TMAPTS·H ₃) ^g		13.3	
Pd(TMAPTS·Na ₃)		-11.1	
Palladacycle 8	24.3		
	14.5		
Palladacycle 12	21.1		
	15.1		
		47.9	22.7
		40.3	16.0
Ar = 2,4-Me ₂ -5-[SO ₃] ⁻ -C ₆ H ₂			

^a Experimentally determined chemical shifts in 2:1 D₂O/CH₃CN unless noted. ^b Calculated with the BLYP exchange–correlation functional. See text. ^c Calculated with the B3LYP exchange–correlation functional. See text. ^d DMF solvent. ^e Obtained at -80 °C in toluene-*d*₆. ^f THF solvent. ^g Non-hydrogen-bonded structure.

results say about the relative steric demand of TXPTS and TMAPTS under the catalytic conditions? The strong charge repulsion experienced by the L³⁻ structures in the gas phase would be less significant in solution where counterions and hydrogen bonding with the solvent would partially mask the negative charges. The L·H₃ and L·Na₃ were calculated to lessen the influence of the charge repulsion, but the presence of sodium ions and protons also induces structural effects due to intramolecular coordination of the sodium and proton between the sulfonate groups in the TPPTS and TMAPTS structures. In an aqueous solution, the sodium or hydrogen ion as well as the sulfonate would be solvated by water. Therefore, the ligands would likely not adopt the same conformation seen in the gas phase. The “true” structure of the ligands is probably intermediate to the trianion and sodium salt structures. The sulfonic acid

(94) Wolinski, K.; Hinton, J. F.; Pulay, P. *J. Am. Chem. Soc.* **1990**, *112*, 8251–8260.

(95) Urata, H.; Suzuki, H.; Moro-oka, Y.; Ikawa, T. *J. Organomet. Chem.* **1989**, *364*, 235–244.

structures are less relevant to the catalytic results, which were carried out under basic conditions. Although much more challenging computationally, it will be of future interest to calculate the $\text{Pd}(\text{L}^{3-})$ and $\text{Pd}(\text{L} \cdot \text{Na}_3)$ structures with shells of water molecules and solvated counterions to more closely simulate the real environment in which these complexes are found and used. A conclusion that can be drawn from these results is that the cone angle, and thus catalytic performance, could be affected by the choice of counterion and solvent medium.

On the basis of the CO stretching frequency of the *trans*- $\text{Rh}(\text{L})_2(\text{CO})\text{Cl}$ complexes, no measurable difference in the electron-donating ability of the sulfonated phosphines could be determined. The sulfonated phosphines were considerably less electron-donating than PPh_3 or $\text{P}(o\text{-tol})_3$ on the basis of these measurements. Comparison with nonsulfonated ligands is complicated, however, by the dependence of the CO stretching frequency on the local environment (solvent, ions, etc.), in addition to the inherent electronic properties of the ligands. In contrast, the computational results show that the sulfonated phosphines do have different electronic properties. For example, if we compare the charge on phosphorus for either the free or bound ligands, we see that $\text{TPPTS} \cdot \text{Na}_3$ has a more positive charge than does PPh_3 , which suggests that PPh_3 is a better electron donor than $\text{TPPTS} \cdot \text{Na}_3$. $\text{TXPTS} \cdot \text{Na}_3$, which has two electron-donating methyl groups, has a less positive charge than $\text{TPPTS} \cdot \text{Na}_3$ or PPh_3 , although it is more positive than the P of $\text{P}(o\text{-tol})_3$. Interestingly, $\text{TMAPTS} \cdot \text{Na}_3$ has a more positive P atom than does $\text{TXPTS} \cdot \text{Na}_3$, which suggests that the inductive withdrawing effect of the methoxy group has a larger effect on the phosphorus charge than its resonance-donating ability. This effect was not observed in the nonsulfonated analogues (TXP and TMAP), however.

All three sulfonated ligands have lower (more negative) HOMO energies than the nonsulfonated ligands for both the free and Pd-bound ligands. Higher energy HOMOs are more available to react, thus PdL complexes with higher energy HOMOs are expected to be more reactive toward oxidative addition. Of the Pd complexes (PdL) of the sulfonated ligands, the HOMO energy trend is $\text{Pd}(\text{TPPTS} \cdot \text{Na}_3) < \text{Pd}(\text{TXPTS} \cdot \text{Na}_3) < \text{Pd}(\text{TMAPTS} \cdot \text{Na}_3)$, all of which have lower energy HOMOs than $\text{Pd}(\text{PPh}_3)$. Thus based on the HOMO energy levels, $\text{TMAPTS} \cdot \text{Na}_3$ is a better electron donor than $\text{TXPTS} \cdot \text{Na}_3$, while both are significantly more electron donating than $\text{TPPTS} \cdot \text{Na}_3$. This trend was mirrored in the case of the nonsulfonated analogues: $\text{PPh}_3 < \text{TXP} < \text{TMAP}$. The opposite trend was observed in the case of the sulfonic acid derivatives, however. The HOMO energy level of the $\text{Pd}(\text{TXPTS} \cdot \text{H}_3)$ was found to be at higher energy than that of the $\text{Pd}(\text{TMAPTS} \cdot \text{H}_3)$ complex, while $\text{TPPTS} \cdot \text{H}_3$ had the lowest PdL HOMO energy.

Overall, the computational results show that $\text{TXPTS} \cdot \text{Na}_3$ and $\text{TMAPTS} \cdot \text{Na}_3$ are better electron donors than $\text{TPPTS} \cdot \text{Na}_3$ and are comparable to PPh_3 . These results are in contrast to what is seen experimentally using the CO stretching frequency of *trans*- $\text{Rh}(\text{L})_2(\text{CO})\text{Cl}$, where all three sulfonated ligands are much less electron donating than PPh_3 . The fact that all three ligands gave identical CO stretching frequencies is surprising. Tolman reported a 2.3 cm^{-1} difference in the CO stretch of the $\text{Ni}(\text{CO})_3\text{L}$ complexes of PPh_3 and $\text{P}(o\text{-tol})_3$.⁵² Since the CO stretch of the rhodium system is more sensitive to ligand electronics, we would expect to see a difference between the methylated (TXPTS and TMAPTS) and nonmethylated (TPPTS) ligands. Given

the large counterion effects seen in the computation results, it is possible that ion-pairing effects in the *trans*- $\text{Rh}(\text{L} \cdot \text{TBA}_3)_2(\text{CO})\text{Cl}$ complexes have a strong effect on the CO stretching frequency. We have previously seen that the TBA counterions in *trans*- $\text{Rh}(\text{TPPTS} \cdot \text{TBA}_3)_2(\text{CO})(\text{NO}_3)$ cluster tightly around the metal center in CH_2Cl_2 , preventing displacement of the nitrate anion.⁹⁶ A similar tight clustering in this CO study may have had a dominating effect on the CO stretching frequency, making the electronic contribution of the phosphine inconsequential.

Palladium Coordination Chemistry. The coordination chemistry of $\text{TXPTS} \cdot \text{Na}_3$ and $\text{TMAPTS} \cdot \text{Na}_3$ with palladium is more complex than that of $\text{TPPTS} \cdot \text{Na}_3$. Differences were also observed in the coordination chemistry of $\text{TXPTS} \cdot \text{Na}_3$ and $\text{TMAPTS} \cdot \text{Na}_3$, despite their similar structural and electronic characteristics. Coordination of $\text{TXPTS} \cdot \text{Na}_3$ with $\text{Pd}(\text{OAc})_2$ did not produce a Pd^0 complex or generate $\text{TXPTS} \cdot \text{Na}_3$ even after standing for 24 h at room temperature, in contrast to Amatore's results with $\text{TPPTS} \cdot \text{Na}_3$.⁶⁷ Amatore⁹⁷ has reported that tri(*o*-tolyl)phosphine will not reduce $\text{Pd}(\text{OAc})_2$, presumably due to the large cone angle that inhibits attack by acetate on the phosphine,⁶⁹ so the lack of reduction by $\text{TXPTS} \cdot \text{Na}_3$ is not necessarily surprising.

When $\text{Pd}(\text{OAc})_2$ was complexed with $\text{TXPTS} \cdot \text{Na}_3$, two major Pd complexes are observed, along with several other minor components. One was a single resonance at 19.5 ppm and the second is an AB pattern with a $^2J_{\text{P,P}}$ coupling of 506 Hz. On the basis of this very large coupling constant, we have concluded that the AB pattern is due to a palladacycle complex (**8**, Figure 9) formed by C–H activation of one of the *ortho*-methyl groups of the ligand. These types of complexes are well precedented for *ortho*-methyl-substituted arylphosphines.^{72,73,75,76} The 19.5 ppm resonance is likely to be due to a complex with the general formula $\text{Pd}(\text{TXPTS} \cdot \text{Na}_3)_n\text{L}_m$ ($\text{L} = \text{H}_2\text{O}$, OH^- , CH_3CN , **7**), although the exact structure of this complex, along with the other minor species present, could not be determined. This cluster of peaks remained essentially the same as the $\text{TXPTS} \cdot \text{Na}_3$:Pd ratio was varied. The same species were also observed when Na_2PdCl_4 was used as the precursor, along with new resonances corresponding to chloride complexes.

$\text{TXPTS} \cdot \text{Na}_3$ is a much less efficient reductant of $\text{Pd}(\text{OAc})_2$ than is $\text{TPPTS} \cdot \text{Na}_3$. While $\text{TPPTS} \cdot \text{Na}_3$ reduces Pd^{II} to Pd^0 efficiently at room temperature without additional reagents, $\text{TXPTS} \cdot \text{Na}_3$ does not form Pd^0 complexes in the absence of other reagents. Traces of $\text{Pd}^0(\text{TXPTS} \cdot \text{Na}_3)_2$ (**11**) were formed in the presence of large excesses of sodium carbonate, but elevated temperatures were required to form **11** in significant amounts. Use of phenylboronic acid as an external reductant increased the rate of reduction, but several hours were required to form **11** as the major species in solution. The $\text{Pd}^0(\text{TXPTS} \cdot \text{Na}_3)_2$ complex could be formed as the major species in solution on a time scale that is comparable to the catalytic reactions at 50 °C in the presence of sodium carbonate or phenylboronic acid and sodium carbonate. The slow formation of the PdL₂ complex at room temperature may explain the low activity of the $\text{TXPTS} \cdot \text{Na}_3$ catalyst system below 50 °C.

In addition to palladacycle **8**, palladacycle **12** could be formed under two different sets of conditions. Complex **12** could be

(96) Sliker, M. D.; P'Pool, S. J.; Traylor, R. K.; McNeil, J., III; Young, S. H.; Hoffman, N. W.; Klingshirn, M. A.; Rogers, R. D.; Shaughnessy, K. H. *J. Organomet. Chem.* **2005**, *690*, 3540–3545.

(97) Amatore, C.; Jutand, A. *Acc. Chem. Res.* **2000**, *33*, 314–321.

prepared along with other products when **11** was treated with phenyl iodide. Alternatively, complexation of TXPTS·Na₃ with Pd(OAc)₂ in the presence of excess phenylboronic acid in the absence of sodium carbonate gave **12** as the main phosphorus-containing species in solution. Since a phenyl source is required to form **12**, we propose that it is a phenyl-substituted analogue of **9** ([Pd(κ^2 -C,P-TXPTS³⁻)(κ -P-TXPTS³⁻)Ph]Na₆). Formation of **12** in the presence of PhB(OH)₂ would involve phenylation of **7** by phenylboronic acid and the activation of an *ortho*-methyl group. Alternatively, palladacycle **12** could be prepared by phenyl transfer to **8**. Formation of **12** by the reaction of phenyl iodide with Pd(TXPTS·Na₃)₂ (**11**) presumably involves oxidative addition, C–H activation, loss of HI, and coordination of a second equivalent of TXPTS·Na₃, although the order of these steps has not been determined.

The coordination chemistry of TMAPTS·Na₃ is similar to that of TXPTS·Na₃, although it binds more strongly to Pd and is a more effective reductant of Pd^{II} than is TXPTS·Na₃. In the reaction of TMAPTS·Na₃ with Pd(OAc)₂ in the presence of sodium carbonate (20 equiv), Pd⁰(TMAPTS·Na₃)₂ (**14**) was the major species present along with Pd^{II}(TMAPTS·Na₃)₂ (**13**). No free TMAPTS·Na₃ was observed in this reaction. Under these same conditions, TXPTS·Na₃ gave an analogous Pd^{II} complex (**7**), but only a trace of a Pd⁰ complex (**11**) after sitting overnight. Furthermore, free TXPTS·Na₃ was always present in significant amounts when large excesses of carbonate were present. It is interesting that TMAPTS·Na₃ coordinates more readily and is a more effective reductant of Pd(OAc)₂ than TXPTS·Na₃, despite their similar electronic and structural properties.

Amatore has suggested that P(*o*-tol)₃ does not reduce Pd(OAc)₂ due to steric hindrance of attack by acetate on the Pd-bound phosphorus.⁶⁸ It is possible that a similar scenario may play a role here, depending on which of our calculated structures is more representative of the solution-state structure. The cone angle of Pd(TMAPTS³⁻) was 16° smaller than the corresponding TXPTS³⁻ complex, while the cone angles for the trisodium salts were within 2°. The calculated cone angle of TMAPTS·Na₃ may be overly large due to the need to accommodate coordination of each sodium ion to two sulfonate groups. In aqueous solution, TMAPTS may adopt a conformation in which it is less hindered than TXPTS. In this scenario, Pd-bound TMAPTS would be able to coordinate more readily and be more susceptible to attack by acetate than TXPTS, leading to reductive elimination.

When the Pd⁰(TMAPTS·Na₃)_n complex was treated with phenyl iodide, an AB pattern very similar to that seen in the case of TXPTS·Na₃ was observed. This same complex was formed in the reaction of TMAPTS·Na₃ with Pd(OAc)₂ in the presence of sodium carbonate and phenylboronic acid. In analogy with the TXPTS·Na₃ complex (**12**), we propose that the AB pattern corresponds to [Pd(κ^2 -C,P-TMAPTS³⁻)(κ -P-TMAPTS³⁻)Ar]Na₆ (**15**, Ar = Ph, 4-ethylphenyl). The palladacycle complex was observed as a major species under catalytic conditions, which suggests that it may be a resting state along the catalytic pathway or a byproduct that siphons off palladium from the catalytic cycle.

Attempts to isolate the complexes derived from TXPTS·Na₃ or TMAPTS·Na₃ have been unsuccessful, which has limited our ability to fully characterize these structures. ¹H and ¹³C NMR spectroscopy of the species formed *in situ* have also been largely uninformative due to the fluxional nature of these complexes and the fact that a mixture of species is generally present. With the exception of the free ligands and their oxides,

the ¹H and ¹³C NMR are dominated by broad peaks that provide little structural information. Spectra obtained at higher and lower temperature show changes in peak shape, but the resonances remain broad over the temperature range accessible in aqueous acetonitrile. Calculated ³¹P NMR chemical shifts of the proposed structures were insufficiently precise to provide insight into the structures observed by NMR. Higher accuracy calculations will be required in order to confirm or disprove the proposed structures.

Catalysis. TXPTS·Na₃ and TMAPTS·Na₃ both gave catalysts that are more active for the Suzuki and Sonogashira couplings of aryl bromides at 50 °C than the catalyst derived from TPPTS·Na₃. TXPTS·Na₃ also gives effective catalysts for the Heck coupling of aryl bromides, while the catalyst derived from TMAPTS·Na₃ has similar activity to the TPPTS·Na₃-derived catalyst. The reason for the lower activity of the TMAPTS·Na₃-derived catalyst compared to the TXPTS·Na₃/Pd(OA)₂ system is not clear, given they have similar structural and electronic characteristics.

The increased activity of the TXPTS·Na₃- and TMAPTS·Na₃-derived catalysts can be attributed to the increased steric demand and electron-donating ability of these ligands compared to TPPTS·Na₃. Both *ortho*-methylated ligands are significantly more sterically demanding than TPPTS·Na₃, which allows them to more readily form highly active PdL-active species. Computational results also show that TXPTS·Na₃ and TMAPTS·Na₃ are stronger electron donors than TPPTS·Na₃. For example, the HOMO energy levels for the PdL complexes of TXPTS·Na₃ and TMAPTS·Na₃ are lower than that of the Pd(TPPTS·Na₃) complex. Higher energy HOMO orbitals would be expected to be more reactive reducing agents in the oxidative addition step.

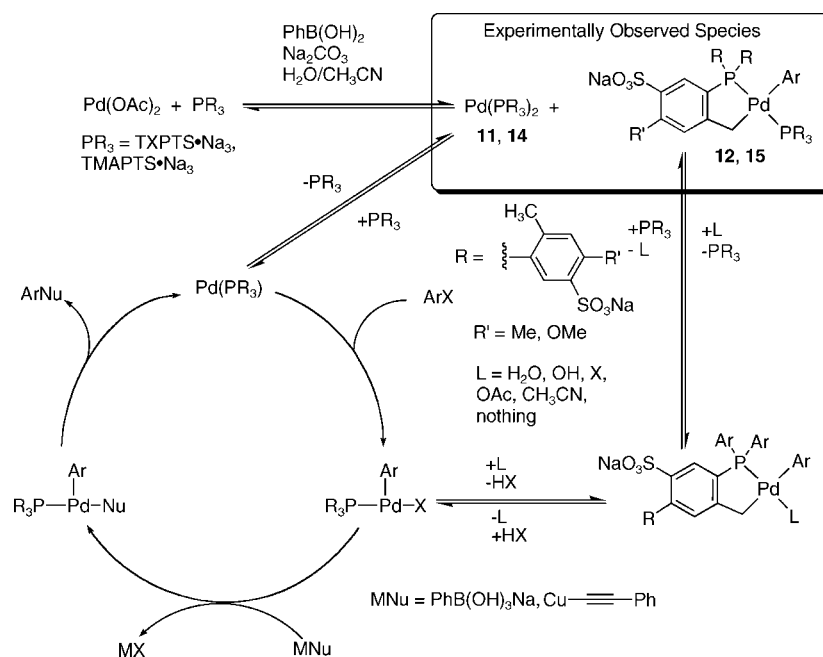
In order to rationalize catalyst activity in terms of ligand properties, it is necessary to establish that the proposed Pd-ligand species is the true active species. It has been established for many systems, particularly those carried out at elevated temperatures (>100 °C), that colloidal palladium clusters are the true active catalysts.^{98–100} The nature of the active species is certainly a relevant question in these systems. In particular, TXPTS·Na₃, which was the most effective ligand for the catalytic reactions tried, appeared to bind weakly to Pd and was slow to promote reduction to Pd⁰ at room temperature. Under catalytically relevant temperatures (50 °C), Pd⁰ complexes were formed readily, however. Therefore, it is possible that **11** and **14** are the catalyst resting states and direct precursors to a Pd⁰L (L = TXPTS·Na₃ or TMAPTS·Na₃) active species. Alternatively, it could be argued that **11** and **14**, as well as the other species observed by ³¹P NMR spectroscopy, are catalytically irrelevant.

For each of the coupling reactions, we saw no activity in the absence of ligand. In addition, the ligand identity had a significant effect on catalyst efficiency. Therefore, we can conclude that the ligand plays a role, although these results do not necessarily require that the active species be a monomeric PdL complex. The effect of aryl halide substrate structure on catalyst activity can also provide circumstantial evidence regarding the identity of the active species. Palladium colloids are generally highly effective with aryl iodide and activated aryl bromide substrates, but tend to be much less active with

(98) de Vries, J. G. *Dalton Trans.* **2006**, 421–429.

(99) Phan, N. T. S.; Van Der Sluys, M.; Jones, C. W. *Adv. Synth. Catal.* **2006**, *348*, 609–679.

(100) Köhler, K.; Kleist, W.; Pröckl, S. S. *Inorg. Chem.* **2007**, *46*, 1876–1883.

Scheme 3. Proposed Catalytic Cycle Based on ^{31}P NMR Spectroscopic Observations

deactivated aryl bromides and chlorides.⁹⁸ With these less active substrates, ligand-free catalysts typically require elevated temperatures, although a ligand-free catalyst system has recently been reported to give high activity for Suzuki couplings of aryl bromides at room temperature.¹⁰¹ Catalysts derived from TXPTS·Na₃ and TMAPTS·Na₃ show good activity with deactivated aryl bromides under relatively mild conditions (50–80 °C).

In an effort to more directly probe the identity of the active catalyst, we have carried out a mercury(0) poisoning test on the TXPTS·Na₃/Pd(OAc)₂ system in the Suzuki coupling of 4-bromotoluene and phenylboronic acid. Mercury(0) readily forms amalgams with heterogeneous metal particles, such as palladium, that are catalytically inactive. Thus, deactivation of a catalyst system upon addition of Hg⁰ provides evidence for the active species being ligand-free metal particles or colloids.³⁹ The mercury test has been applied to a number of palladium pincer complexes used as precatalysts in cross-coupling reactions.^{102–105} In each case, catalyst activity was completely or significantly inhibited when Hg⁰ was added to the reaction mixture, which was interpreted as evidence for palladium colloids being the true active species. In our system, addition of a large excess of Hg⁰ had no effect on the rate of product formation when it was added at the beginning or in the middle of a catalytic reaction. Addition of Hg⁰ at the beginning of the reaction should have resulted in no activity if colloidal palladium was the true active species, since these colloids would have been deactivated by Hg⁰ as they were formed. Addition of mercury after the reaction had started would have stopped the catalytic reaction if it was catalyzed by colloidal palladium. The fact that no inhibition was observed suggests that a phosphine-bound,

monometallic species (PdL) is the true active species rather than colloidal palladium particles. We cannot conclusively exclude the possibility that a phosphine-free complex or colloid, which is unaffected by Hg⁰, is the true active species, however.

In cross-coupling reactions employing palladium catalysts derived from sterically demanding phosphine ligands, the active species is generally thought to be a monophosphine palladium species that is in equilibrium with a Pd⁰L₂ resting state (Scheme 3). The mercury experiments are consistent with soluble Pd-phosphine complexes being the true active species, rather than colloidal palladium. Therefore, the phosphine complexes observed by NMR spectroscopy may be catalytically relevant. We have observed a Pd⁰L₂ species for both the TXPTS·Na₃ (**11**) and TMAPTS·Na₃ (**14**) prior to the addition of aryl iodide. When an aryl iodide is added to provide a complete catalytic system, complex **14** remains present in the TMAPTS·Na₃ system, while **11** is completely consumed in the TXPTS·Na₃ system. For both ligands, the Pd($\kappa^2\text{C},P\text{-L}$)($\kappa P\text{-L}$)Ph complex (L = TXPTS·Na₃ (**12**), TMAPTS·Na₃ (**15**)) was present in significant amounts after the aryl iodide was added.

Although palladacycle complexes are widely used as precatalysts,¹⁰⁶ the majority of evidence in the literature suggests that they are not catalytically viable.^{98,107,108} Most commonly, they are thought to be precursors to palladium colloids, although they can also act as precursors to ligand-bound Pd⁰ species.¹⁰⁹ On the basis of this prior evidence, we believe that palladacycles **12** and **15** are side products formed in the catalytic cycle. It is possible that **12** and **15** serve as resting states from which catalytically active species can be regenerated. Alternatively, they may represent unproductive side processes that consume the active catalyst.

(101) Deng, C.-L.; Guo, S.-M.; Xie, Y.-X.; Li, J.-H. *Eur. J. Org. Chem.* **2007**, 1457–1462.

(102) Yu, K.; Sommer, W.; Weck, M.; Jones, C. W. *J. Catal.* **2004**, *226*, 101–110.

(103) Bergbreiter, D. E.; Osburn, P. L.; Frels, J. D. *Adv. Synth. Catal.* **2005**, *347*, 172–184.

(104) Eberhard, M. R. *Org. Lett.* **2004**, *6*, 2125–2128.

(105) Nilsson, P.; Wendt, O. F. *J. Organomet. Chem.* **2005**, *690*, 4197–4202.

(106) Dupont, J.; Consorti, C. S.; Spencer, J. *Chem. Rev.* **2005**, *105*, 2527–2571.

(107) Beletskaya, I. P.; Cheprakov, A. V. *J. Organomet. Chem.* **2004**, *689*, 4055–4082.

(108) Böhm, V. P. W.; Herrmann, W. A. *Chem.–Eur. J.* **2001**, *7*, 4191–4197.

(109) d'Orlyé, F.; Jutand, A. *Tetrahedron* **2005**, *61*, 9670–9678.

We propose that the catalytic cycle proceeds in a similar fashion to others proposed for sterically demanding ligands with complexes **11** and **14** acting as direct precursors to the Pd⁰L active catalyst.

Conclusion

TXTPS·Na₃ and TMAPTS·Na₃ are sterically demanding, air-stable hydrophilic phosphines that provide effective catalysts for aqueous-phase Suzuki and Sonogashira couplings of aryl bromides under mild conditions. Moreover, they are more easily prepared in high purity than TPPTS·Na₃. TXPTS·Na₃ also gives an active catalyst for the aqueous-phase Heck coupling, while the catalyst derived from TMAPTS·Na₃ was much less effective. These ligands provide significantly more active catalysts than the commonly used TPPTS·Na₃. Computational studies of these ligands were complicated by their polyanionic nature. Large structural changes were observed as a function of the presence and identity of the sulfonate counterion. These effects suggest that choice of solvent and counterion may play a role in the steric demand of these ligands. The computational results show that TXPTS·Na₃ and TMAPTS·Na₃ are significantly more sterically demanding than TPPTS·Na₃. The *ortho*-methylated ligands are also predicted to be somewhat more electron donating than TPPTS·Na₃, a feature that could not be ascertained from measurement of metal–carbonyl stretching frequencies. On the basis of the computational studies on the properties of these ligands, we conclude that the increased activity observed for catalysts derived from TXPTS·Na₃ and TMAPTS·Na₃ compared to TPPTS·Na₃ is due primarily to the significantly larger cone angles of TXPTS·Na₃ and TMAPTS·Na₃. The increased electron-donating ability of these ligands also likely contributes to the improved catalytic activity seen with these ligands compared to the less electron-donating TPPTS·Na₃.

Complexation studies showed that Pd(OAc)₂ was reduced very slowly by TXPTS·Na₃ at room temperature, even in the presence of phenylboronic acid. In contrast, TMAPTS·Na₃ reduced Pd(OAc)₂ more rapidly. Both ligands gave PdL₂ complexes upon reduction of the palladium salt. Palladacycle complexes were identified on the basis of ³¹P NMR spectral data for both ligands. Both the PdL₂ and palladacycle complexes were observed under catalytically relevant conditions. The PdL₂ species is presumed to be the direct precursor of the active PdL species, while it is unclear if the palladacycle serves as a resting state or is an unproductive side reaction that consumes the active catalyst.

Experimental Section

General Comments. TXPTS·Na₃ and TMAPTS·Na₃ were prepared as previously described.^{35,36} All other materials were obtained from commercial suppliers and used as received. Water (deionized) and aqueous acetonitrile solutions were deoxygenated by sparging with nitrogen for at least 15 min before each use.

Representative Procedure for the Suzuki Cross-Coupling Reactions. Pd(OAc)₂ (5.60 mg, 0.025 mmol), ligand (0.063 mmol), arylboronic acid (1.20 mmol), and Na₂CO₃ (0.210 g, 2.00 mmol) were added to a 50 mL round-bottom flask equipped with a stir bar and rubber septum while in the drybox. Upon removing the flask from the drybox, the aryl bromide (1.00 mmol) and deoxygenated 1:1 CH₃CN/H₂O (10 mL) were added via syringe. The reaction was placed in a preheated oil bath at 50 or 80 °C and allowed to stir until determined to be complete by GC (typically 2–4 h). The reaction mixture was poured into saturated sodium carbonate (50 mL), extracted with ethyl acetate (3 × 30 mL), and dried with MgSO₄.

The crude products were purified by flash chromatography (SiO₂).

Representative Procedure for the Sonogashira Cross-Coupling Reactions. Pd(OAc)₂ (8.8 mg, 0.03 mmol) and ligand (0.08 mmol) were added to a 50 mL round-bottom flask equipped with a stir bar and rubber septum while in the drybox. Upon removing the flask from the drybox, the aryl bromide (1.00 mmol), diisopropylamine (242 mg, 2.40 mmol), degassed 1:1 CH₃CN/H₂O (10 mL), and alkyne (1.20 mmol) were added via syringe. For the best conversion the alkyne should be added last. The reaction was placed in a preheated oil bath and allowed to stir until determined to be complete by GC. The reaction was poured into saturated sodium carbonate (50 mL), extracted with ethyl acetate (3 × 30 mL), and dried with MgSO₄. The crude products were purified by flash chromatography (SiO₂).

Representative Procedure for the Heck Coupling Reactions with Styrene. Pd(OAc)₂ (5.60 mg, 0.025 mmol), TXPTS·Na₃ (43.7 mg, 0.075 mmol), and Na₂CO₃ (212 mg, 2.00 mmol) were added to a 50 mL round-bottom flask equipped with a stir bar and rubber septum while in the drybox. Upon removing the flask from the drybox, the aryl halide (1.00 mmol), styrene (156 mg, 1.50 mmol), and degassed 1:1 CH₃CN/H₂O (10 mL) were added via syringe. The round-bottom flask was placed in an oil bath at 80 °C and allowed to stir until complete (GC). The reaction mixture was poured into saturated sodium carbonate (50 mL), extracted with ethyl acetate (3 × 30 mL), and dried with MgSO₄. The crude products were purified by flash chromatography (SiO₂).

Representative Procedure for the Heck Coupling Reactions with Sodium Acrylate. The coupling was carried out as described above for styrene, but using sodium acrylate (141 mg, 1.50 mmol) as the alkene. Upon consumption of the starting materials, the reaction mixture was added to a saturated solution of sodium carbonate (50 mL). The residual aryl bromide was extracted with ethyl acetate (3 × 30 mL). The pH of the aqueous phase was then brought to ca. 1 using concentrated H₂SO₄. The cinnamic acid product was extracted with CH₂Cl₂ (3 × 30 mL), and the combined organic extracts were dried over MgSO₄. Removal of solvent under reduced pressure gave the crude product, which was recrystallized from H₂O/ethanol.

General Procedure for Synthesis of Ligand TBA Salts. The sodium salt of the trisulfonated ligand (0.17 mmol) was placed in a flask with tetrabutylammonium chloride (167 mg, 0.60 mmol). Water (4 mL) was added and the clear solution allowed to stir for 1 h. The mixture was extracted with methylene chloride. Removal of solvent gave viscous oils that solidified after drying under vacuum (0.1 Torr). The products were used without further purification.

General Procedure for Measurement of Ligand Electronic Parameters. Solutions of L₂Rh(CO)Cl complexes were synthesized according to the procedure reported by Vastag.⁶³ The phosphine (0.050 mmol), trimethylamine *N*-oxide (0.020 mmol), and [Rh(CO)₂(μ-Cl)]₂ (0.010 mmol) were added to a vial equipped with a stirbar and septa while in the drybox. Upon removing the vial from the drybox 1 mL of distilled methylene chloride was added to the reaction vessel via a syringe and the reaction mixture was allowed to stir for 1 h. At this time a sample of the reaction solution was transferred to an air-free solution cell (NaCl windows) via a disposable syringe. Rh(PPh₃)₂(CO)Cl: 1979 cm⁻¹, Rh(TXPTS·(TBA)₃)₂(CO)Cl: 1993 cm⁻¹; Rh(TMAPTS·(TBA)₃)₂(CO)Cl: 1993 cm⁻¹; Rh(TPPTS·(TBA)₃)₂(CO)Cl: 1993 cm⁻¹.

General Procedure for Ligand Complexation Studies. Pd(OAc)₂ (2.2 mg, 0.01 mmol), ligand (0.025–0.05 mmol), Na₂CO₃ (0–1 mmol), and PhB(OH)₂ (0–0.05 mmol) were combined in a small, septum-sealed vial in the drybox. The vial was removed from the box and attached to a nitrogen manifold

by a needle. Deoxygenated 2:1 D₂O/acetonitrile (1 mL) was added to the vial via syringe. After mixing to dissolve all of the solids, a portion of this solution (0.4 to 0.5 mL) was transferred via syringe to an NMR tube that had been sealed under nitrogen with a septum. Samples were analyzed by ³¹P{¹H}, ¹H, or ¹³C{¹H} NMR spectroscopy immediately after preparation and then periodically over a period of several hours.

Acknowledgment. Financial support for this work by the National Science Foundation (CHE-0124255), the School of Mines and Energy Development at The University of Alabama, Chemical Sciences, Geosciences and Biosciences Division, Office of Basic Energy Sciences, U.S. Department of Energy (DOE) (catalysis center program), the Robert Ramsay Chair Foundation, The

University of Alabama Graduate School (fellowship for E.C.W.), and the NSF-funded REU program at The University of Alabama (summer fellowship for K.P.O.) is gratefully acknowledged. We thank Dr. Kenneth Belmore and Dr. Russell Timkovich for assistance with the NMR experiments reported in this paper.

Supporting Information Available: Detailed experimental data, product characterization data, calculated optimized molecular geometries in Å, as well as total and zero-point energies in au, and NMR spectra from the complexation studies. This material is available free of charge at <http://acs.pubs.org>.

OM7008606